STATIC AND DYNAMIC COMPRESSION LOAD TESTS OF CONICALLY CONNECTED, SCREW FIXED DENTAL ABUTMENT – IMPLANT ASSEMBLIES

[1]Győző Körtvélyessy, [2]Dávid Botond Hangyási, [1]Tamás Tarjányi, [3]Zsolt Tóth, [4]Danica Matusovits, [4,†]István Pelsőczi-Kovács and [4,†]Zoltán Baráth

[1]Department of Oral Biology and Experimental Dental Research, Faculty of Dentistry, University of Szeged, Tisza Lajos krt. 64-66, 6720 Szeged, Hungary;
[2]Department of Periodontology, Faculty of Dentistry, University of Szeged, Tisza Lajos krt. 64-66, 6720 Szeged, Hungary;
[3]Department of Medical Physics and Informatics, Albert Szent-Györgyi Medical School, Faculty of Science and Informatics, University of Szeged, Korányi fasor 9, 6720 Szeged, Hungary;
[4]Department of Prosthodontics, Faculty of Dentistry, University of Szeged, Tisza Lajos krt. 64-66, 6720 Szeged, Hungary;

E-mail addresses: kortvelyessy.gy@gmail.com, tarjanyi.tamas@stoma.szote.u-szeged.hu, hangyasi.david@stoma.szote.u-szeged.hu, ztoth@physx.u-szeged.hu, matusovitsdanica@gmail.com, pelsoczi.istvan@stoma.szote.u-szeged.hu, barath.zoltan@stoma.szote.u-szeged.hu
† These authors contributed equally to this work.

ABSTRACT

The key for the long-term success of dental implants is the mechanical stability of the implant and the abutment anchored in it. The conical connection between screwed dental implants and abutments has good mechanical stability. However, with long-term use of the dental restoration fixed on a dental implant in the oral cavity, mechanical deformation of the assembled abutment in the implant and loosening of the fixing screw often occur, which affects long-term functionality. To study these processes, static compression loading tests were performed with various conical angle connections (35°, 55°, 75° and 90°) using Grade 4 and 5 titanium implant materials. After loading the implant and abutment assemblies with up to 500 N, the resulting deformations in length and diameter as well as the reverse-torque of the fixing screw were measured. No significant differences were observed between the results when the tested implant and abutment material was either Grade 4 or 5. Additionally, dynamic compression tests were performed on Grade 4 samples with different conical angles (30°, 45° and 60°). The relative changes in length (strain) of the assembly were determined over 30,000 cycles due to force varying periodically between 100 and 400 N. The reverse torques were also measured after the dynamic loading. The static and dynamic compression tests showed the same trend for different cone angles. Impression of the abutment into the dental implant was observed for lower conical angle connections. On the other hand, lower strain values were observed at larger conical angles. The reverse torque values of the fixing screws were only the half of the forward torque in case of lower conical angles, while high stability was observed with the larger conical angle connections (~ 20-30% reduction in torque). In summary, it is recommended to use a higher angle of the conical connection in order to avoid larger deformations in the lengths and diameters of the assembled implant and abutment system, as well as a significant reduction in the torque of the fixing screw.

Keywords: titanium implant; dynamic load; static load; conical angle, implant-abutment connection, screw loosening

1. INTRODUCTION

Titanium (Ti) has become a commonly used alloplastic material, due to its excellent biomechanical properties. Dental implants, which are used to replace missing tooth roots, have been performing well in clinical applications for decades [1]. Implant supported fixed partial dentures provide a similar aesthetic appearance to natural teeth and the restorations anchored on implants have no detrimental effect on adjacent teeth [2]. The load transmission mechanism of dental implants is considerably different from that of natural teeth, where periodontal ligaments play an important role in the stress-absorbing capacity [3]. Stress

reduction – similar to that of periodontal ligaments – is not present in osseointegrated implants, and therefore occlusal loads are transmitted directly to the jaw bone. The daily loading in the oral environment leads to micro-movements in the connection, reversible then irreversible changes in the shape of the implant, micron-sized ruptures and then fractures in the implant and the connected elements, in addition to bone resorption, which may lead to peri-implant bone defects and even implant loss [4, 5]. Therefore, application of an appropriate implant-abutment connection and mechanical testing prior to clinical application is of paramount importance. The relationship between the implant and the abutment is usually described as an internal or external relationship. The distinguishing factor separating the two groups is the presence or absence of a geometric element extending above the coronal surface of the implant. The connection may also be described as a sliding fit, where there is a small space between the mating parts and the connection is passive, or a friction fit, where there is no space between the mating parts and the parts are literally forced together. The mating surfaces may include rotational resistance and indexing and/or lateral stabilizing geometry. This geometry is hereafter described as octagonal, hexagonal, tapered, tapered hexagonal, cylindrical hexagonal, spindle, cam, cam tube and pin/spigot. New generation implants mostly have an internal conical connection, although the angle of taper varies substantially. From a mechanical aspect there is still no clear determination about the ideal taper angle for the implant-abutment connection.

Grade 4 (commercially pure Ti) and Grade 5 Ti are commonly used materials for dental implants, although there are pronounced differences between their mechanical properties. Grade 4 Ti is a relatively soft and ductile metal, which makes it easy to machine and shape into dental implants. Grade 4 Ti has a lower tensile strength than Grade 5 Ti, however it is still strong enough for most dental applications and has a higher biocompatibility compared to Grade 5 Ti [6]. Grade 5 Ti (Ti-6Al-4V) is an alloy that contains aluminium (Al; ~6%) and vanadium (V; ~4%) is stronger and more durable than Grade 4 Ti. Grade 5 Ti has a higher ultimate tensile strength (~950 MPa) than Grade 4 Ti (~550 MPa). Several publications discuss that Ti raw materials are tough and resistant to plastic deformation [7,8].

The main goal of dental implant design is to achieve efficient bone-shaping-properties required by the bone quality, mechanical stability and ensure a strong bone–to-implant-contact and osseointegration [9]. The implant failure rate due to static and dynamic loads is 32% for implants with inadequate initial stability [10-14]. It is therefore critical to estimate the potential for failure in a given dental implant design. Experimental mechanical testing of dental implants provides useful data for clinicians, physicists and engineers. The load is transmitted from the prosthesis to the implant and surrounding bone. The transmission of forces and stress distribution are influenced by a number of factors, such as occlusion, abutment design, fit and the micromovements of the crown and the abutment, implant-abutment connection, implant platform, thread design at the implant neck, implant body design, number and location of implants, inclination and osseointegration of implants, and finally, the quantity and quality of bone [15].

Static and dynamic mechanical measurements should be performed to estimate the long-term success of a given implant system. The design of the connection should ensure that the reverse torque is not lowered due to the occlusal forces, however, the loosening of the screws is a very common problem [16,17]. In addition to the differences in the raw material and the cone angles, the manufacturing parameters and the dimensional accuracy of the manufactured products also play an important role [18].

The aim of our study was to investigate the mechanical stability of the conical connected dental implant and abutment assemblies with different internal cone angle values, using static and dynamic compression load tests. The following research questions arose in our study: *i) D*oes the value of the cone angle affect the screw loosening due to external forces and what degree of conicity is ideal for mechanical stability? *ii)* How does the material of the implant (grade 4 and 5) influence the mechanical behaviour, do reversible or irreversible deformations of the implants occur? *iii)* What extent the inaccuracy of the taper angles (positive and negative tolerance) affects the geometry of the implant and abutment assemblies? These sets of succeeding questions are not yet systematically investigated.

2. MATERIALS AND METHODS

2.1. Instruments and implant models

Static compression load tests were performed with a self-developed loading machine (Fig. 1), while the dynamic tests were performed with an all-electric dynamic test instrument (Instron ElectroPuls E3000, Norwood, MA, USA).
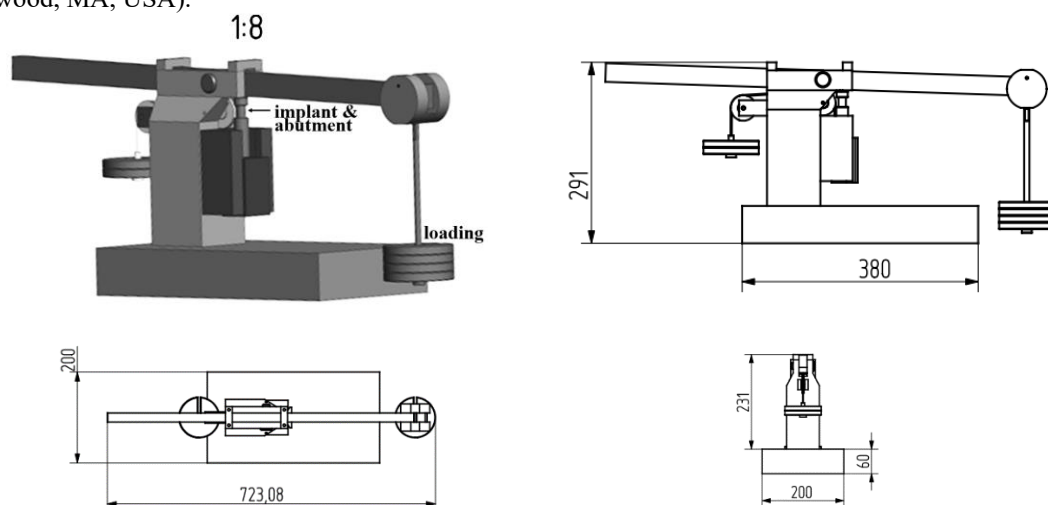

Figure 1. Technical drawings of the loading machine developed by the authors. The one-arm lifter with a lever ratio of 1:8 is loaded by cylinders with a weight of 1.25 kg each. The resulting compression force may be set between 0 N and 500 N.

The implant models and abutments were manufactured by Denti System Ltd. (Szentes, Hungary), an example is shown in Fig. 2. For the static load test, the abutments and implant body models were made from Grade 4 and Grade 5 Ti materials, 3.4 and 3.8 mm in diameter, with the following cone angles: 35°, 55°, 75°, and 90°. A total of n=84 abutment-implant assemblies were used for static load tests with at least 3 samples were tested using the same parameter set. For the dynamic load test abutments and implant bodies were prepared from Grade 4 Ti in 3.4 mm diameter with the following cone angles: 30°, 45° and 60°. A total of n=21 implant samples were used for dynamic load tests. To measure forward and reverse torque values a BMS MS150 electric torque screwdriver (BMS Torque Solutions, Ireland) was used.

Figure 2. Pictures of a test implant and abutment used in the study

2.2. Static load test protocol

Static load tests were performed with a self-developed loading machine at the Faculty of Dentistry, University of Szeged. Static load tests were performed on a minimum of 3 samples per group. At the onset of the protocol, implants and the according abutments were assembled without tightening the fixing screw. The height of this assembly and the diameter of the implant neck were measured and recorded. After this, the fixing screw was fastened with 35 Ncm torque. Static compression loads were then applied. The choice of the load was based on the amount of mastication force applied to a tooth. The specimens were subjected to a successive load increase. The steps were 100-200-300-400-450-500 N (100 N corresponds to 10 kg weight). Each loading step was lasted for 60 s. The lengths of the implant-abutment assemblies were measured after each step of compression. After the 300N and 500 N loading the implant neck diameter was measured again. After completing the static compression load test, the fixing screw connecting the implant to the abutment was untwisted and the extension torque values were measured. The implants and abutment were reassembled without tightening the fixing screw and the total length and diameter were measured. Then the connection was then fixed by tightening the fixing screw to 35 Ncm torque again and the length of the abutment implant assembly was measured. After 60 seconds the fixing screw was tightened again and the reverse torque value was measured after 24 hours.

2.3. Dynamic load test protocol

Dynamic load tests were performed by an all-electric dynamic test instrument (Instron ElectroPuls E3000, Norwood, MA, USA) at the Faculty of Dentistry, University of Szeged (see Fig. 3 for experimental setup). Dynamic load tests were performed on a minimum of 7 samples per group. Based on our previous measurements [19], abutment implant assemblies from Grade IV Ti with different conical angles (30°, 45° and 60°) were included for further fatigue tests. For each assembly, the protocol was initiated with tightening the fixing screw between the abutment and the implant with 35 Ncm torque. Following this, the assemblies were put under loads. In the first phase 250 N load over 10 seconds was applied on the implant abutment. The dynamic load test started after this phase. During the dynamic load test a periodic force with 150 N amplitude sine wave was applied with 15 Hz frequency. This results in a force that varies dynamically over time between 100 N and 400 N. The dynamic compression test lasted 30000 cycles, after which, the 250 N loading force was released over another 10 seconds to 0 N. The device sets the force values over time and records the position of the loading head. From these values compression force-strain graphs can be prepared.
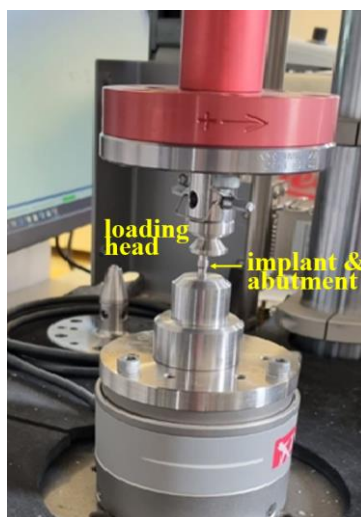
Figure 3. Mechanical fatigue testing machine used during the experiments and the setup of the dynamic load test. The loading head of the machine was perpendicular to the top surface of the implant head.

2.4. Inaccuracies due to manufacturing parameters

The mechanical parameters of the abutment implant models used in the study, as well as their parameter tolerances, have a significant impact on their performance. The abutments and implant models used in our study were designed using the Creo Parametric 5.0 software. As part of our investigation – with the help of this design software – implants and according abutment parts were drawn with the acceptable tolerances of the parameters. With the help of the software the tight fit case of the assembly was compared with the manufactured extreme, but still tolerated fit case. Following this, the length differences were determined between the cases of abutment and implant elements manufactured with the worst tolerance value in the opposite direction and the ideal, precisely sized abutment implant assemblies.

2.5. Statistical analysis

Statistical analysis was performed using Microsoft Excel (Microsoft Corp., Redmond, WA, USA) and SPSS Statistics 23.0 software (IBM Corp., Somers, NY, USA). Descriptive statistics of the measurements were presented as mean ± SEM (standard error of the mean). Linear regression analysis was performed on the measured data with fit equations and coefficient of determination (R^2) values. One-way analysis of variance (ANOVA) followed by Tukey HSD post hoc tests were performed. The significance level was set as 5% ($p<0.05$).

3. RESULTS AND DISCUSSION

3.1. Static load results

During the static mechanical loading tests, the lengths of the abutment implant assemblies were measured after applying 0, 100, 200, 300, 400, 450 and 500 N compression forces; the results of these measurements can be seen in Fig. 4. Overall, no significant differences were shown between the behaviours of implants from Grade 4 and Grade 5 raw materials in the case of connections with different taper angles (35°: $p=0.562$; 55°: $p=0.666$; 75°: $p=0.235$; 90° $p=0.944$). The largest strain was obtained for the 35° angle connections, for both Grade 4 and Grade 5 assemblies, respectively, as can be clearly seen in Fig. 4.
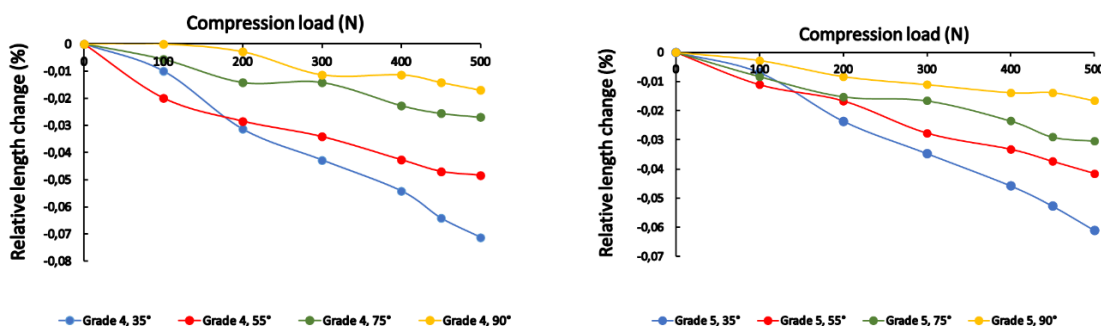

Figure 4. Relative length changes for Grade 4 and Grade 5 Ti implants after different static loads

After the application of 500 N compression load, the reverse torque was measured upon disassembling the implant and abutment parts; the results are presented in Fig. 5., with a comparison of Grade 4 and Grade 5 implants. Overall, reverse torque values consistently increased with the conical angle, i.e., the lower values were observed for the 35° conical angle case, while the highest for the 90° case. On the other

hand, no significant differences were noted when comparing the reverse torque values of Grade 4 and 5 implants with the same conical angle ($p > 0.05$).
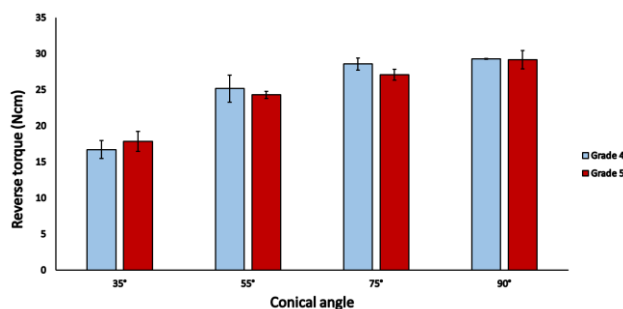

Figure 5. Reverse torque (mean ± SEM) values in case of Grade 4 and Grade 5 Ti implants with different conical angle cases (35°, 55°, 75°, and 90°)

Diameter changes of the implant models corresponding to different loads (0, 300, 500 N) were examined, during which, diameter values were measured at three locations. Figs. 6a-b and Figs. 6c-d show the relative diameter change for the Grade 4 and Grade 5 3.45 mm and 3.8 mm diameter implant models, respectively (where each data point represents the average value of 6 samples). No significant differences were found between the case of the different Ti grades.
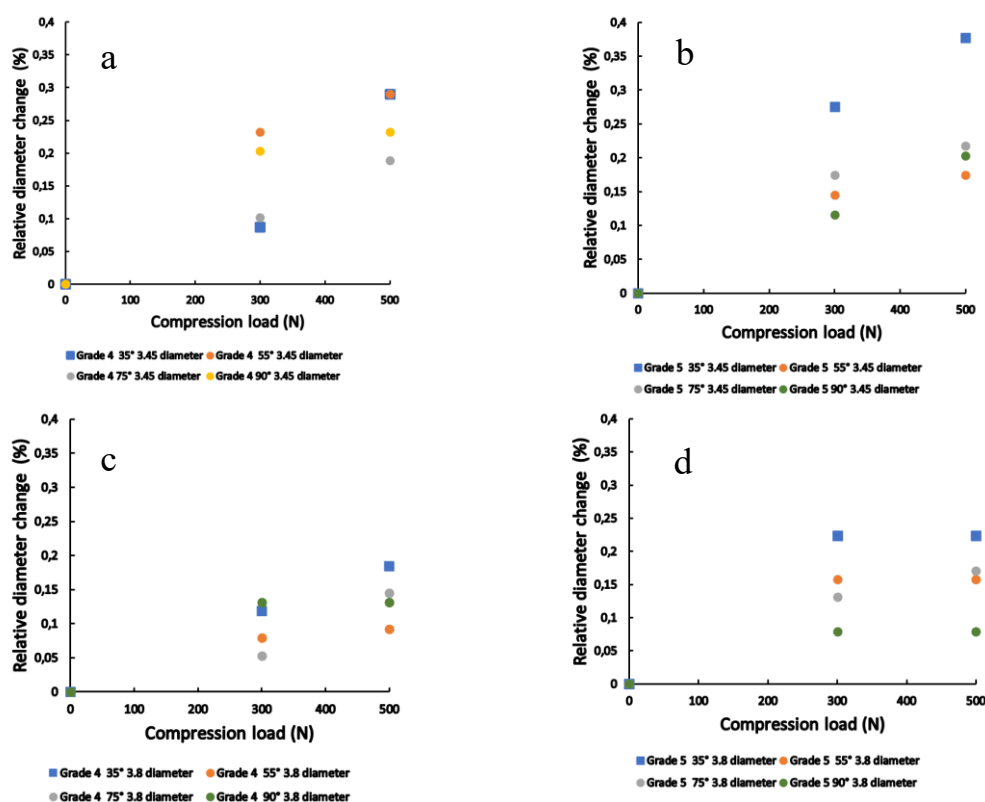
Figure 6. Relative diameter changes of the Grade 4 and Grade 5, Ø 3.45 mm and Ø 3.8 mm Ti implants under different static compression loads, corresponding to the tested internal taper contact angles (35°, 55°, 75°, and 90°)

3.2. Dynamic load results

During the dynamic load test, the fatigue testing machine recorded the loading head position from which, compression strain of the implants with different conical angles (30°, 45° and 60°) can be determined. It was observed that there is a permanent deformation in the material, as the loading and unloading curves did not coincide. However, due to the elastic properties during the unloading phase, the material can still partially recover its length. It was also studied whether there were any differences in the impression of the implant head into the implant body during the fatigue cycles. Fig. 7 indicates that the implant head and the implant moved indeed closer together. The loading-unloading nature of this test revealed that most of the impression occur in the very first cycles, while it remains constant in the subsequent cycles; this is shown as the curves immediately begin to shift to larger displacement values, and after that there is no essential change between the loading-unloading cycles. Thus, the samples suffered elastic deformation mainly after this early phase.
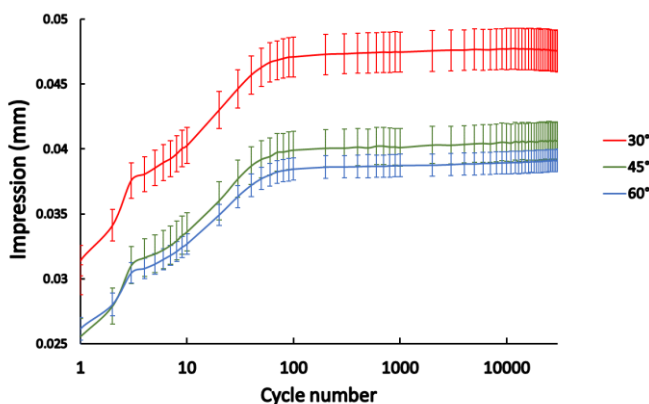

Figure 7. Mean impression levels of the implant head into the implant over the dynamic load test cycles. Sampling was carried out more frequently in the early phase of the test, while in the later stages, sampling was done in every 1000 cycles.

Final displacement values – indicating irreversible impressions of the abutments into the implant bodies – were also measured with the dynamic testing machine, following the dynamic test, as shown in Fig. 8. The highest impression value was measured for the 30° case (0.047± 0.002 mm), while the lowest value was found in the 60° case (0.039±0.001 mm), respectively; observed differences between the conical angle groups were statistically significant ($p<0.001$).
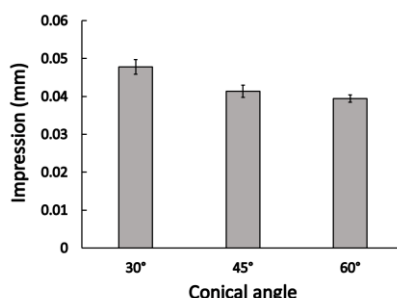
Figure 8. Displacement values (mean ± SEM) measured for each conical angle group (30°, 45° and 60°) after the fatigue test

After the dynamic loading test, reverse torque values were also measured upon disassembling the implant head and implant body; the resulting reverse torque values are shown in Fig. 9. Similar observations were obtained to our previous measurement, the lowest torque values were shown in for the 30° conical angle case, while the highest were seen for 60°; significant differences were noted among the mean reverse torque values; significant differences were observed between the average torque (p=0.003) in case of 30° (18.7 ± 1.01 Ncm), 45° (21.25 ± 0.67 Ncm) and 60° (24.03 ± 0.59 Ncm). Additionally, based on post hoc test, a significant difference between the 30° and 60° conical connections (p=0.043) was verified, while this was not the case for the 30° vs. 45° and 45° vs. 60° comparisons.
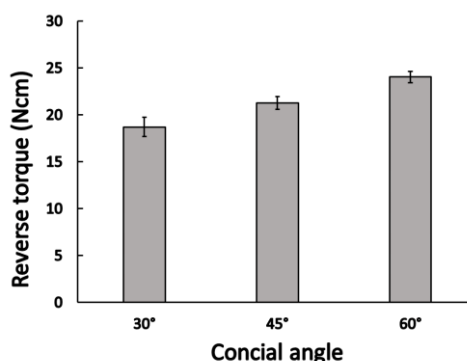

Figure 9. Reverse torque (mean ± SEM) measured for each conical angle group (30°, 45° and 60°) upon disassembling the implant head and implant after the fatigue tests

3.3. Inaccuracies due to manufacturing parameters

For the implants in our samples, a taper angle tolerance of +0/-0.5° was accepted; however, during the production of the samples, we strived to be close to 0 degrees. For the abutments, the same tolerance of 0/+0.5° was acceptable (see Fig. 10).
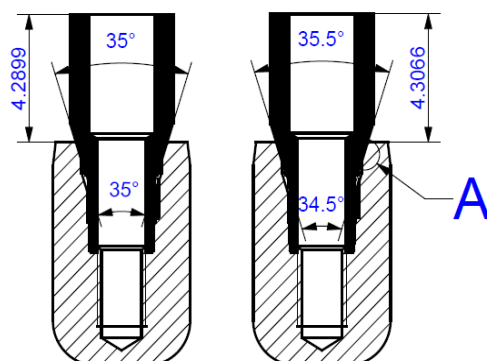
Figure 10. Schematic drawing of the conical implant and abutment head, marked with the angles and lengths.

Adjusting the tolerances in the worst possible mating, we determined the height differences from the perfectly fitting assembled abutment and implant parts, which are summarized in Table 1.

Table 1. Implant abutment height difference for conical angles with opposite tolerances for the abutment and implant parts

Ideal connection angle	Negative tolerance of the implant cone angle	Positive tolerance of the abutment cone angle	Resulting height difference from ideal connection [mm]
24°	23.5°	24.5°	0.0271
35°	34.5°	35.5°	0.0167
55°	54.5°	55.5°	0.0071
75°	74.5°	75.5°	0.0041
90°	89.5°	90.5°	0.003

From the results presented in Table 1. it can be seen, that the height of the assembled abutment and implant differs from the optimal situation if one suspects the errors resulting from the negative tolerance of the implant and positive tolerance of the abutment cone angles. As the cone angle increases the height difference decreases significantly. This calculation serves with an explanation about the reasons of the measured phenomena, namely that applying higher conical angles results in lower impressions (c.f. Fig. 8.)

3.4. Discussion, Clinical relevance of results

In our study, both the static and dynamic measurements showed similar results. Conical closure was clearly visible in the case of the implant-abutment connection with different tapers. There is also a dependence in the case of the reverse torque, i.e., the larger the cone angle of the connection, the greater the reverse torque value we measured. The static measurements resulted in that the smaller the cone angle between the implant and the abutment, the greater the diameter increase of the implant at the conical closure under load. As a result, the mechanical stress value of the implant body on the bone will be higher, i.e., more stress is transferred to the bone, which may lead to increased bone resorption rates.

T. Paepoemsin *et al.* conducted a study in which the removal torque of three different types of fixing screws was evaluated after mechanical cyclic loading [20]. In their paper, they worked with flat head and conical screws, and then compared the reverse torques of each group after 1 million cycles after the first 10 minutes of dynamic loading. When comparing the measured reverse torque with the results of the first 10-minute dynamic load test and after 1 million cycles, a significant decrease was shown. Our results also

indicated that a change occurred during the dynamic loading test that reduced the tension of the implant abutment head.

Benjaboonyazit *et al.* also studied the formation of loose connections due to fatigue [21]. In their report, 3.75 mm Octatorx taper implants were used and the screws were tightened to 30 Ncm, followed by a very long dynamic loading test of 2 million cycles, and then the removal torque values were compared. Their results are also consistent with our results, i.e. they obtained a reverse torque value of over 27 Ncm without load, which decreased to below 16 Ncm after their fatigue test protocol. Our study showed that the reduction of the reverse torque can be moderated with an increased taper angle. Comparing the static 55° results, which resulted in a reverse torque of 24-25 Ncm, after the dynamic load test, the 60° case decreased to very similar values, i.e. around 24 Ncm. These results also highlighted that increasing the taper angle does indeed promote stronger grip for longer periods of time, even under intermittent loads.

Joo-Hee and Hyun-Suk also performed cyclic loading on Grade 4 Ti implants with an external hexagonal connection [22]. Following the ISO protocol, the implants were inserted at an angle of 30°. After 1 million cycles, the reverse torque was measured at 15.2 Ncm at 300 N (equivalent to 30 kg); we also determined the torque values before the dynamic test, which was 25.2 Ncm. Their results coincide with the results of the present study, in their case the reduction of the reverse torque was approximately 40% compared to the pre-post dynamic test. The referenced articles support the results of our tests, i.e. under loading, the greater the angle of the implant-abutment-connection was, the smaller the amount of screw loosening could be measured.

Screw loosening of taper-connected implants (i.e., a loose state of the clip between the implant and the fixing screw) may be an important clinical problem, as it increases the risk of denture removal and screw failure. Screw loosening of implants may be due to various reasons, such as incorrect tension of the screw, excessive load on the screw, a defect in the material or size of the fixation screw, wear between the implant and the fixation screw, or continuous slippage of the screw due to continuous loading. Therefore, properly securing the implant and fixing screw and inspecting the abutment stability in the implant by the dentists is critical. Reversible and irreversible shape deformations of Ti implants may have a significant impact on the success of the implant surgery and the long-term stability of the implant. In reversible deformation, deformation occurs during surgery or subsequent loading (mastication) due to the elasticity of the Ti implant, but the implant returns to its original shape when the load is removed. This type of shape deformation is usually associated with micro- and macro-deformations due to loading, which may lead to fatigue fracture in the long term. During irreversible shape deformation, the implant does not return to its original shape, even after the load is removed; this is usually due to exceeding the yield point or excessive deformation during surgery. Irreversible deformation may have a serious effect on the stability of the implant, as the shape of the implant changes and, as a result, the implant does not fit properly with the implant bed. In order to prevent irreversible deformity, dentists must be careful to choose the right size and shape of implant and carefully plan and perform surgical procedures. Planning, with pre-planning and simulation, plays an important role in selecting the right sized and shaped implants for the patient and ensuring the correct fit of the implant to the implant bed. Performing professional procedures and using appropriately chosen implants may reduce the risk of irreversible shape deformations and improve the long-term stability of the implants. The inaccuracy of the taper angles of the implant and the abutment has a considerable influence on the compression under load. The greater the dimensional error from manufacturing, the greater the impression of the abutment into the implant body along the conical surfaces.

In this research, a systematic study was performed to investigate the role of the conical angle during static and dynamic load tests. Furthermore, the influence of the implant and abutment material (i.e. Grade 4 and 5) was also investigated in case of static compression measurements. During the investigations, we compared the influence of the angle of conical connections on the reverse torque values. To the best of our knowledge, such publication was not yet published, where these parameters were comprehensively assessed. The results found in the literature partially overlap with ours, but did not cover all parameters of our investigations.

4. CONCLUSIONS

In this study, mechanical testing of assembled abutments and implants demonstrated that increasing the conical angle of the connection decreases permanent strain values. Static compression experiments revealed that there are no significant differences in reverse torque between Grade 4 and Grade 5 abutment and implant assemblies that share the same conical angle. In summary, it is recommended to use a connection with a higher taper angle in order to avoid major deformations of the lengths and diameters of the implant at the connection and a significant reduction in the torque of the fixing screw. Our results may contribute to understanding the long-term success of dental implants.

5. ACKNOWLEDGEMENTS

REFERENCES

[1] H.J. Haugen, H. Chen, 2022. Is There a Better Biomaterial for Dental Implants than Titanium? - A Review and Meta-Study Analysis. J. Funct. Biomater. 13: e46. https://doi.org/10.3390/jfb13020046

[2] G. Ustaoglu, D. G. Bulut, Z. U. Aydin, 2022. The Effect of Single-Tooth Implant Restorations on Prognosis of Adjacent Teeth and on Fractal Dimension of Peri-Implant Trabecular Bone: A Retrospective Study. Selcuk Dent. J. 9: 208-215. https://doi.org/10.15311/selcukdentj.920654

[3] C. Pandey, D. Rokaya, B.P. Bhattarai, 2022. Contemporary Concepts in Osseointegration of Dental Implants: A Review. BioMed Res. Int. 2022: e6170452. https://doi.org/10.1155/2022/6170452

[4] L. Bing, T. Mito, N. Yoda, E. Sato, R. Shigemitsu, J. M. Han, K. Sasaki, 2020. Effect of peri-implant bone resorption on mechanical stress in the implant body: In vivo measured load-based finite element analysis. J. Oral Rehabil. 47: 1566-1573. https://doi.org/10.1111/joor.13097

[5] D.T. Száva, A. Száva, J. Száva, B. Gálfi, S. Vlase, 2022. Dental Implant and Natural Tooth Micro-Movements during Mastication-In Vivo Study with 3D VIC Method. J. Pers. Med. 12: e1690. https://doi.org/10.3390/jpm12101690

[6] C.L. de Andrade, M.A. Carvalho, D. Bordin, W.J. da Silva, A.A.B. Cury, B.S. Sotto-Maior, 2017. Biomechanical Behavior of the Dental Implant Macrodesign. Int. J. Maxillofac. Implants 32: 264-270. https://doi.org/10.11607/jomi.4797

[7] G.A. Zarb, A. Schmitt, 1990. The longitudinal clinical effectiveness of osseointegrated dental implants: the Toronto study. Part III. Problems and complication encountered. J. Prosthet. Dent. 64: 185-194. https://doi.org/10.1016/0022-3913(90)90177-e

[8] P. Vigolo, F. Fonzi, Z. Majzoub, G. Cordioli, 2006. An in vitro evaluation of titanium, zirconia, and alumina procera abutments with hexagonal connection. Int. J. Oral. Maxillofac. Implants 21: 575-80.

[9] Á.L. Nagy, Z. Tóth, T. Tarjányi, N.T. Práger, Z.L. Baráth, 2021. Biomechanical properties of the bone during implant placement. BMC Oral Health 21: e86. https://doi.org/10.1186/s12903-021-01442-1

[10] C. Cumbo, L. Marigo, F. Somma, G. La Torre, I. Minciacchi, A. D'Addona, 2013. Implant platform switching concept: a literature review. Eur. Rev. Med. Pharmacol. Sci. 17: 392-397.

[11] R. J. Lazzara, S.S. Porter, 2006. Platform switching: a new concept in implant dentistry for controlling postrestorative crestal bone levels. Int. J. Periodontics Restorative Dent. 26: 9-17.

[12] I. S. Moon, T. Berglundh, I. Abrahamsson, E. Linder, J. Lindhe, 1999. The barrier between the keratinized mucosa and the dental implant. An experimental study in the dog. J. Clin. Periodontol. 26: 658–63. https://doi.org/10.1034/j.1600-051x.1999.261005.x

[13] S. Elleuch, H. Jrad, A. Kessentini, M. Wali, F. Dammak, 2021. Design optimization of implant geometrical characteristics enhancing primary stability using FEA of stress distribution around dental prosthesis. Comp. Methods Biomech. Biomed. Engineering 24: 1035-1051. https://doi.org/10.1080/10255842.2020.1867112

[14] O. Camps-Font, L. Rubianes-Porta, E. Valmaseda-Castellón, R.E. Jung, C, Gay-Escoda, R. Figueiredo, 2021. Comparison of external, internal flat-to-flat, and conical implant abutment connections for implant-supported prostheses: A systematic review and network meta-analysis of randomized clinical trials. J. Prosthet. Dent. https://doi.org/10.1016/j.prosdent.2021.09.029

[15] Y. Kuang-Ta, H. Kao, C.K. Cheng, H.W. Fang, M.L. Hsu, 2019. Mechanical performance of conical implant-abutment connections under different cyclic loading conditions. J. Mech. Behav. Biomed. Mater. 90: 426–432. https://doi.org/10.1016/j.jmbbm.2018.10.039

[16] A. S. Vinhas, C. Aroso, F. Salazar, P. López-Jarana, J.V. Ríos-Santos, M. Herrero-Climent, 2020. Review of the Mechanical Behavior of Different Implant–Abutment Connections. Int. J. Environ. Res. Public Health, 17: e8685. https://doi.org/10.3390/ijerph17228685

[17] C. M. Chu, H.L. Huang, J. T. Hsu, L. J. Fuh, 2012. Influences of internal tapered abutment designs on bone stresses around a dental implant: three-dimensional finite element method with statistical evaluation. J. Periodontol. 83: 111-118. https://doi.org/10.1902/jop.2011.110087

[18] M. Karl, TD. Taylor, 2014. Parameters determining micromotion at the implant-abutment interface. Int. J. Oral Maxillofac. Implants. 29: 1338-47. https://doi.org/10.11607/jomi.3762

[19] G. Körtvélyessy, Á.L. Szabó, I. Pelsőczi-Kovács, T. Tarjányi, Z. Tóth, K. Krisztina, D. Matusovits, B.D. Hangyási, Z.L. Baráth, 2023. Different Conical Angle Connection of Implant and Abutment Behavior: A Static and Dynamic Load Test and Finite Element Analysis Study. Materials 16: e1988. https://doi.org/10.3390/ma16051988

[20] T. Paepoemsin, P.A. Reichart, P. Chaijareenont, F.P. Strietzel, P. Khongkhunthian, 2016. Removal torque evaluation of three different abutment screws for single implant restorations after mechanical cyclic loading. Oral Implantol. 9: 213-221. https://doi.org/10.11138/orl/2016.9.4.213.

[21] K. Benjaboonyazit, P. Chaijareenont, P. Khongkhunthian, 2019. Removal torque pattern of a combined cone and octalobule index implant-abutment connection at different cyclic loading: an in-vitro experimental study. Int J Implant Dent 5: e1. https://doi.org/10.1186/s40729-018-0154-2

[22] Joo-Hee Lee, Cha. Hyun-Suk, 2018. Screw loosening and changes in removal torque relative to abutment screw length in a dental implant with external abutment connection after oblique cyclic loading. J. Adv. Prosthodont. 10: 415-421. https://doi.org/10.4047/jap.2018.10.6.415

THE EXISTENCE OF GLUTEN-FREE AND FUNCTIONAL PASTA IN HUNGARY

Szűcs Krisztián

Naturtrade Hungary Kft. H-6725, Szeged, Szabad Sajtó u. 54.

ABSTRACT

Nowadays, instead of traditional wheat grains, alternative cereals, also known as pseudocereals, are increasingly coming to the fore. The reason for this is, among other things, that more and more people struggle with food allergies and intolerances. Gluten-related disease - such as gluten sensitivity - is a chronic disease of the small intestine with malabsorption, which is triggered by gluten, a vegetable protein found in certain cereals, in people who are sensitive to it. Because of this, the demand for foods in which alternative gluten-free pseudocereals play a prominent role has understandably increased. Our research and development goal was aimed at getting to know and examining the different raw materials and their functional enrichment possibilities, which has led to the development of a new range of pasta products.

INTRODUCTION

Wheat appeared, about 10,000 years ago in the so-called „fertile crescent" of Southeast Asia (present-day Turkey, Palestine, Lebanon and northern Iraq). Wheat cultivation dates back to the beginning of agriculture, when various wild cereals, including wheat and barley, appeared spontaneously [1].

Wheat/gluten-related diseases can be divided into three different disorders: autoimmune, allergic and neither autoimmune nor allergic.

The term gluten is used to describe wheat proteins (prolamins and glutenins). However, other cereals also have proteins that have toxic effects on patients with celiac disease: toxic prolamins include gliadin in wheat, secalin in rye and hordein in barley. For a time, oats were excluded from the celiac diet because it was believed that avenin (a protein in oats) was also toxic to patients. In addition, the use of oats in gluten-free diets is still controversial due to possible cross-contamination with gluten containing cereals.

Coeliac disease is a chronic autoimmune disease caused by a persistent intolerance to gluten proteins. Many people think that celiac disease is more like a multisystemic immunological disorder than a disease confined to the gastrointestinal tract. The clinical symptoms of the disease vary widely and depend on the age of the patient and the duration of the disease. An important feature of the disease is the absence of enzymatic digestion of gliadin fragments in the gastrointestinal tract.

Wheat allergy is characterised by an IgE and non-IgE mediated immune response, which in some individuals results in an allergic reaction when touching or inhaling foods containing wheat. However, IgE cross-reactivity to other cereals is also possible in some individuals.

Patients with non-celiac gluten sensitivity (NCGS) are referred to as having neither autoimmune nor allergic disease. They have the same symptoms as celiac disease but test negative for it. Patients with coeliac disease should follow a strict gluten-free diet as they should avoid foods containing gluten, patients with wheat allergy should avoid contact with all forms of wheat and patients with NCGS should also follow a wheat/gluten-free diet [2].

Wheat grains contain three main components, which are separated by milling: bran, germ and endosperm, which makes up 70-72% of the total grain and contains the toxic components. The storage proteins of cereals can be divided into two main groups: the ethanol-soluble fraction known as prolamins and the polymeric glutenins. The prolamins from different cereals are called differently, wheat prolamins are called gliadin, rye prolamins are called secalin, barley prolamins are called hordein and oats prolamins are called avenin [3][4]. The only effective and safe treatment for the disease is a strict gluten-free diet, which must be completely free of wheat, rye, barley and triticale. Ancient wheat varieties such as kamut and spelt should also be avoided as they are genetically similar to modern wheat and have a similar amino acid profile. The diet also includes the exclusion of potential cross-contamination. Many other crops are safe for people with celiac disease, the best known being rice and maize [5]. However, in recent years, interest in the gluten-free diet has increased dramatically and more and more people are following it, including those who do not suffer from any of the three diseases.

The list of cereals, grains, seeds, seeds, legumes and nuts that can replace gluten is quite long (including, for example, quinoa, millet, sorghum and chickpeas). These can all improve the diversity of a gluten-free diet, but they are rarely used, partly because of their higher cost and lower availability. Processed foods based on amaranth, quinoa and buckwheat are higher in protein, fat, fibre and minerals than those based on rice and maize, and can be good alternative ingredients for gluten-free products [6].

Individuals with coeliac disease tend to compensate for the restrictions of a gluten-free diet by consuming foods high in fat, sugar and calories, and therefore an overconsumption of total fats and saturated fats is observed in coeliac patients. For this reason, it is advisable to regulate their diet with the help of a specialist, who will provide guidelines on macro- and micronutrients. Intakes of complex and simple carbohydrates should account for about 55% of total calories. A wide range of pulses, alternative cereals and seeds are allowed. In recent years the nutritional composition of small cereals and pseudo-grains has been characterised and shown to be a good source of carbohydrates, dietary fibre, minerals and vitamins. They are also higher in protein content and of better quality than wheat. Dietary fibre is a complex mixture of plant materials that is resistant to digestion. Several studies have shown that a diet high in fibre can prevent many human diseases, such as colon cancer and diabetes. Protein intake should account for about 15% of total calories. The main dietary protein sources in a gluten-free diet are foods of animal origin such as meat, milk and dairy products, eggs and fish. Among plant-based raw materials, legumes, nuts, seeds and gluten-free cereals are useful sources of protein. Total fat intake should account for no more than 25-30% of total calories. Preference should be given to monounsaturated and polyunsaturated fat intakes. These can be found in foods such as vegetable oils, nuts, seeds and fish with higher fat content (e.g. salmon). In contrast, intakes of saturated fats, which are mainly found in foods of animal origin (red meat, poultry, dairy products), should be limited [2].

People who are allergic or intolerant to gluten can mainly eat foods that are naturally gluten-free (e.g. fruits, vegetables, meats). Since gluten eliminates many of the foods that play an important role for them, they replace them with gluten-free substitute foods (pasta, bread, cereals), in which wheat flour is replaced by gluten-free flours [7].

The popularity of pasta is growing worldwide, thanks to its convenience, taste and long and easy shelf life. In addition to the traditional pasta products made from durum wheat semolina, pasta is usually enriched with certain cereals (e.g. barley, rye), pseudo-grain (e.g. buckwheat, amaranth, quinoa) and leguminous flours (e.g. peas, chickpeas, etc.) to provide a source of fibre, minerals, antioxidants and polyphenols [8]. Leguminous flours are also excellent because they increase nutritional value by providing beneficial high protein, fibre and vitamin content, as well as having positive effects on glycaemic response and organoleptic properties [9]. In recent decades, a newer group of pasta products, gluten-free pasta, has been consumed not only by the growing number of people with celiac disease, but also by others who wish to exclude gluten-based products from their diet for health reasons or fashion. Currently, a wide range of products made from

rice, corn and other gluten-free flours are available for people with gluten intolerance. Unfortunately, most of them have poor cooking quality, especially compared to their wheat counterparts. In addition, many gluten-free products are nutritionally inferior, i.e. poorer in minerals and biocomponents, than the wheat-based foods they are intended to replace. Pasta is one of the simplest grain-based products in terms of ingredients and processing. Both raw material characteristics and processing conditions play a key role in determining the quality of the final pasta product. The biggest challenge is therefore gluten-free pasta and bread, as gluten is their basic building block.

Among the gluten-free grains, amaranth, quinoa, teff and buckwheat are becoming increasingly popular, as they improve the nutritional content of gluten-free products in terms of their high fiber content, vitamins, minerals and other bioactive ingredients (polyphenols, phytosterols, etc.). Excellent sources of minerals, especially potassium, iron, calcium, zinc and phosphorus. Their vitamin content is also favorable regarding the B and E vitamin groups. Sorghum is also becoming more and more popular, as it is a good source of protein, starch and antioxidant compounds, which is why it can be used in addition to or as a substitute for corn and rice flours in the preparation of gluten-free foods [7,9].

Manufacturers may also use additives to improve the quality of the pasta. Examples include hydrocolloids, which are generally used because they can form a gel in small quantities, provide high consistency at room temperature and improve firmness. In addition, they can increase the rehydration rate of dough due to their water binding capacity. A wide range of hydrocolloids can be used, including for example xanthan gum, locust bean gum or carboxymethyl cellulose [6]. In addition to the properties mentioned above, these materials are also used as a kind of replacement for the gluten mesh in an attempt to improve the structure of gluten-free products.

The term functional food was first introduced in Japan in the 1980s, and since then it has been used more and more widely until today. This term is defined in several ways, one of which is accepted is that it refers to a processed food that contains ingredients that, in addition to nutrition, can also help certain functions of the body [10]. According to another generally accepted definition, this category includes any food or food ingredient that, in addition to its nutritional value, has a positive effect on an individual's health, physical performance or mental well-being [11].

In recent years, more and more consumers have become aware of functional foods, particularly in the hope that they may offer additional health benefits that can reduce the risk of certain diseases or promote optimal well-being [12]. Food manufacturers have recognised and started to adapt to these growing demands. As a result, functional foods have been developed in almost all food categories, even if they are not equally distributed across all segments of the food industry. As a consequence, consumer preferences may vary from market to market. Among the food markets, functional foods have emerged mainly in dairy products, confectionery, soft drinks, bakery products and baby food. These functional foods can also be classified into separate categories according to their type: there are foods fortified with additional nutrients (e.g. vitamins, minerals), there are fortified foods that contain ingredients not normally found in them (e.g. probiotics), and there are foods from which an ingredient considered harmful to the individual has been removed or reduced and thus makes life easier (e.g. lactose-free, gluten-free).

MATERIALS AND METHODS

The aim of our research was to create a new type of gluten-free pasta family, which have some functional characteristics. In addition to the usual reduced carbohydrate content among pastas, the specific aspect was the development of pasta enriched with protein and minerals. In terms of its base material, in addition to being gluten-free, it was important that it should not be made from rice and corn flour. For this, we turned to several types of different pseudocereals, such as millet, sorghum, quinoa, buckwheat and amaranth. In

addition, we also used oats, teff and psyllium husk as auxiliary materials. These materials were examined from the aspects of shredding, wetting, and water absorption. We examined flour mixtures prepared in different variations for making pasta, which, in addition to the raw material, also involved many modifications of the proportions in the recipe [13]. The finished wet pasta was dried with several drying parameters, which were evaluated by sensory judges after cooking.

A questionnaire survey was also conducted to assess the gluten-free diet.

RESULTS AND DISCUSSION

Based on the results of the questionnaire survey, gluten-free pasta has a right to exist in Hungary and there are still market situations that can be exploited. As a result, the pasta is not only gluten-free, but can also be eaten by people following other diets.

Among the pre-shredding operations, wetting was not necessary in most cases, both because of the already hulled raw materials (e.g. millet) and because of the specific characteristics of the other materials. By varying the speed/time parameters during shredding, it was possible to determine the optimum values for all raw materials and their mixtures. By performing a sieve analysis, we were able to examine several grain sizes during dough production regarding the water absorption of the flours and the behavior of the dough. The ideal grain size was 160 μm, which is very rare for gluten-free flours, so we used a sieve with this coating. The pastas had to be designed to be compatible with a vegan lifestyle, so we used psyllium husk flour, because in this way we can avoid not only eggs, but also other hydrocolloids. Thanks to this, it turned out to be a special task to determine the right amount of psyllium husk flour, since it can thicken even a very small amount, regardless of the water temperature. The recipes for the pastas had to be created with this in mind, adapting all the other flours so that the end result was not a jelly-like mass. The adjustment of this was variable, as the pastas were made from different ingredients. The dry pastas were tested in an accredited laboratory to make sure that our fortification claims comply with current legislation. For the high in protein pasta, this was achieved using green pea protein, while for the carbohydrate-reduced pasta, bamboo fibre was used.

Figure 1: The new Easy Pasta product range

The basis of each pasta recipe was buckwheat, millet and teff flour, except for the low-carb version, as millet had to be omitted due to its high carbohydrate content. For mineral enrichment, selenium was used. We chose selenium because it is recognized as an essential nutrient for humans [14], and its intake varies greatly around

the world, being lower in Europe and higher in the USA. Low levels of selenium have been linked to an increased risk of mortality, poor immune function and cognitive decline. Higher levels of selenium are antiviral and reduce the risk of autoimmune thyroid diseases [15]. Increasing your selenium intake may have long-term health benefits, particularly in reducing the risk of cancer. The initial links between selenium intake and cancer risk came from epidemiological studies that showed an inverse relationship between blood selenium concentrations and the risk of several cancers, primarily in men. In addition to these, selenium can also improve the immune response. It plays a role in supporting the development and expression of all components of the immune system, i.e. non-specific, cell-mediated and humoral immunity. Its deficiency reduces the immune competence, while its replacement to adequate level restores the immune functions impaired by deficiency. At an even higher intake, it increases the immune response [16].

The recommended daily intake value for selenium for adults is 55 µg. The dosage of selenium for the flour mixture was 0.01%, which corresponds to about 8 µg per serving. With this amount, it was possible to achieve that the recommended daily intake value of the selenium remaining in the dry pasta is approx. cover 15%.

CONCLUSIONS

During the research, many raw materials, which are excellent in their own right, were examined from a pasta production point of view, starting with the milling of the flour required for the production of the pasta. Throughout the production process, it was important that the product was gluten-free, so suppliers had to be selected. The raw materials are high-quality pseudo-cereals, from which pasta can be found on the market anyway. The developed pastas are unique in terms of their ingredients and selenium enrichment. Thanks to the technology used during milling, its quality is closer to fine wheat flour than its competitors. This new product range is called Easy Pasta, which also refers to their quick and easy preparation. Three pastas with different properties make up this product range: the high in protein, the carbohydrate reduced and selenium enriched pasta. In terms of their appearence, they are made in the form of fusilli and tagliatelle. These developed pastas are suitable for a wide range of uses and can be incorporated into a variety of diets, as opposed to the general gluten-free pasta, including many special diets. According to the growing trend that has occurred in recent years, there will continue to be a demand for these pastas, because of the increasing number of consumers who may be suffering from gluten sensitivity or other diseases.

REFERENCES

[1] Greco, L. (1997): *From the neolithic revolution to gluten intolerance: benefits and problems associated with the cultivation of wheat*. J Pediatr Gastroenterol Nutr. 1997 May;24(5):S14-6; discussion S16-7. doi: 10.1097/00005176-199700001-00005

[2] Saturni, L., Ferretti, G. & Bacchetti, T. (2010): *The Gluten-Free Diet: Safety and Nutritional Quality.* Nutrients, 2(1), 16–34. doi: 10.3390/nu2010016

[3] Véha A, Szabó P. B., Gyimes E (2012): *Peritec technology to reduce fusarium toxin in the milling technology*, REVIEW OF FACULTY OF ENGINEERING ANALECTA TECHNICA SZEGEDINENSIA pp. 131-136. ISSN 1788-6392

[4] Szabó, P. Balázs; Véha, Antal (2008): *Physico-mechanical properties of winter wheat*, CEREAL RESEARCH COMMUNICATIONS 36 : S2 pp. 1003-1006. , 4 p.

[5] Ciclitira, P. J., Ellis, H. J. & Lundin, K. E. A. (2005): *Gluten-free diet—what is toxic?* Best Practice & Research Clinical Gastroenterology, 19(3), 359–371. doi: 10.1016/j.bpg.2005.01.003

[6] Bascuñán, K. A., Vespa, M. C. & Araya, M. (2016): *Celiac disease: understanding the gluten-free diet.* European Journal of Nutrition, 56(2), 449–459. doi: 10.1007/s00394-016-1238-5

[7] Lee, A. R., Ng, D. L., Zivin, J. & Green, P. H. R. (2007): *Economic burden of a gluten-free diet.* Journal of Human Nutrition and Dietetics, 20(5), 423–430. doi: 10.1111/j.1365-277x.2007.00763.x

[8] Marti, A. & Pagani, M. A. (2013): *What can play the role of gluten in gluten free pasta?* Trends in Food Science & Technology, 31(1), 63–71. doi: 10.1016/j.tifs.2013.03.001

[9] Pellegrini, N. & Agostoni, C. (2015): *Nutritional aspects of gluten-free products.* Journal of the Science of Food and Agriculture, 95(12), 2380–2385. doi: 10.1002/jsfa.7101

[10] Kaur, S. & Das, M. (2011): *Functional foods: An overview*. Food Science and Biotechnology, 20(4), 861–875. doi: 10.1007/s10068-011-0121-7

[11] Goldberg, I. (1994): *Functional Foods: Designer Foods, Pharmafoods, and Nutraceuticals. An Aspen Publication*, Chapman and Hall, London, UK. pp. 3-4

[12] Bigliardi, B. & Galati, F. (2013): *Innovation trends in the food industry: The case of functional foods.* Trends in Food Science & Technology, 31(2), 118–129. doi: 10.1016/j.tifs.2013.03.006

[13] Balázs P. Szabó (2013): *Kernel hardness and dough reological investigation on different wheat varieties*, REVIEW OF FACULTY OF ENGINEERING ANALECTA TECHNICA SZEGEDINENSIA 2013:(1-2) p. 59. (2013)

[14] Combs, G. F. Jr. (2001): *Selenium in global food systems*. Br J Nutr 85:517–547.

[15] Rayman, M. P. (2012): *Selenium and human health*. The Lancet, 379(9822), 1256–1268. doi: 10.1016/s0140-6736(11)61452-9

[16] Finley, J. W. (2007): *Increased intakes of selenium-enriched foods may benefit human health*. Journal of the Science of Food and Agriculture, 87(9), 1620–1629. doi:10.1002/jsfa.2943

MERGE IN THE ETHEREUM BLOCKCHAIN – TECHNOLOGY DEVELOPMENT IN A NEW AND INNOVATIVE INDUSTRY

[1] András Bertalan, [2]Balazs Gyenge, [3]Károly Kacz

[1]Széchenyi István University, Vár 2., 9200, Mosonmagyaróvár, Hungary, e-mail: bertalan.andras@sze.hu
[2]Hungarian University of Agriculture and Life Sciences, Páter Károly 1., 2100 Gödöllő, Hungary, e-mail: gyenge.balazs@uni-mate.hu
Széchenyi István University, Vár 2., 9200, Mosonmagyaróvár, Hungary, e-mail: kacz.karoly@sze.hu

ABSTRACT

The food industry has been at the forefront of rapid implementation for several technological innovations. One of the main reasons for this is that food security has been of paramount importance in supplying a growing population, taking into account both quantitative and qualitative requirements. And the necessary development could only be ensured by incorporating the latest developments.

Blockchain technology is also a tool to consider in terms of how it can help track food chains. Its widespread application is only a decade old, but in some areas, for example, the operation of cryptocurrencies has already accumulated enough experience to see if it really lives up to the hopes attached to it, and what problems still stand in the way of further spread. With this material, our primary goal is to present a significant technological change that aims to solve one of the main problems of blockchain-based data management. It will be presented how the technology works (with a specific focus on the proof of work mechanism) and the transition to a truly significant platform, the proof of stake mechanism at Ethereum. This gives us an idea of how much a relatively new technology can undergo changes, and at what rate a seemingly significant problem (in this case, e.g. environmental impact) can decrease. This potential for development provides the basis for counting blockchains as a technology that can be applied in other areas, such as the food industry. In addition to scientific treatises, we often rely on Internet sources in the material, since the change occurred so quickly that publications in scientific journals could not yet track it or only in a narrower circle.

Keywords: blockchain, environmental impact.

1. INTRODUCTION

Blockchain technology has been widely used in the case of cryptocurrencies, with Bitcoin developers being the first to use it to keep the ledger of digital currency. However, its development can be dated to earlier [1]. University of Berkeley (California) doctoral student David Chaum outlined a blockchain database in his dissertation "Computer Systems Established, Maintained, and Trusted by Mutually Suspicious Groups" [2]. Decentralized databases existed before, but he is considered the inventor. Chaum also wanted to use the technology for business, for which he founded a business called DigiCash in 1989. He also created his own cryptocurrency called eCash, however, the business could not be commercially successful, so he later ceased to exist [3].

Blockchain is actually a database, which differs from traditional solutions in that information is stored not on a server (i.e. a centralized network), but on a distributed network [4].

In the case of centralized networks, such as banks or agencies, our data is managed centrally, which requires a strong level of trust in their direction. This is necessary because the data handled in this way is exposed to serious dangers, since if there is a problem with the central storage, either due to intentional damage or failure, the entire database can be compromised. The source of such a problem can be a hacker attack, a natural disaster, the abuse of the registry keeper, etc. In the case of a decentralized network, these problems do not arise, since information is available in several places and its modification is possible only at the cost of extremely great efforts, which in practice means the impossible.

The best example of decentralized networks is the Internet itself. When we connect to the ISP with our phone, tablet or computer to reach a larger provider, we are practically using a decentralized network.

In the case of blockchain, information is downloaded to computers operating on nodes of distributed networks. Its operation is provided by pre-written software that is immutable and tamper-proof. If there is a database change, such as a transfer, it is checked by software running on all computers on the network, and then its database is updated.

As previously mentioned, the use of blockchain technology in the case of cryptocurrencies has become widespread. This is because, even in the case of traditional national currencies, serious confidence is required to operate the system. It is necessary to trust the Central Bank that it will not degrade the value of the currency, which has already happened in history for most currencies. It is necessary to trust commercial banks to store, manage and carry out transactions of funds deposited with them. However, this process is also known to not operate one hundred percent, since bank failures have already occurred, suffice it to think of the bankruptcy of Lehmann Brothers in 2008.

From the foregoing, it is clear that the blockchain architecture, due to its operation, is suitable for being used to track various supply chains. So is, it meets the requirement of reliability, since the information recorded during the process cannot be modified, and even if an error occurs during the recording, the correction is also carried out only with a new block, that is, the data originally recorded can also be seen. This data is accessible to all actors in the food chain, so all participants can be accountable and their activities can be monitored in the process. As a result, the journey of food from farm to fork can be tracked in real time [5]. The latter fact gives the other great advantage, since if there is a problem with the product, it is possible to very quickly delimit the range of products and trace the source.

2. PROOF OF WORK ALGORITHMS

The proof of work algorithm is presented through the solution used for the Bitcoin cryptocurrency, since the mechanism of operation is the same, so an implemented example can be suitable for real illustration.

In the process, the players in the Bitcoin payment network, the so-called mining computers, have to perform a mathematical calculation, which requires significant computing power. So, there is a cost to perform the calculation (computational capacity), so not everyone is able to produce data. At the same time, if the result of the mathematical operation has already been calculated, then the rest of the network can quickly and easily verify that the result is real. In the case of Bitcoin, mathematical operations are designed in such a way that on average there is a result every 10 minutes, such this way, a block can be created every 10 minutes, which is connected to the last block of the blockchain network (Fig. 1).
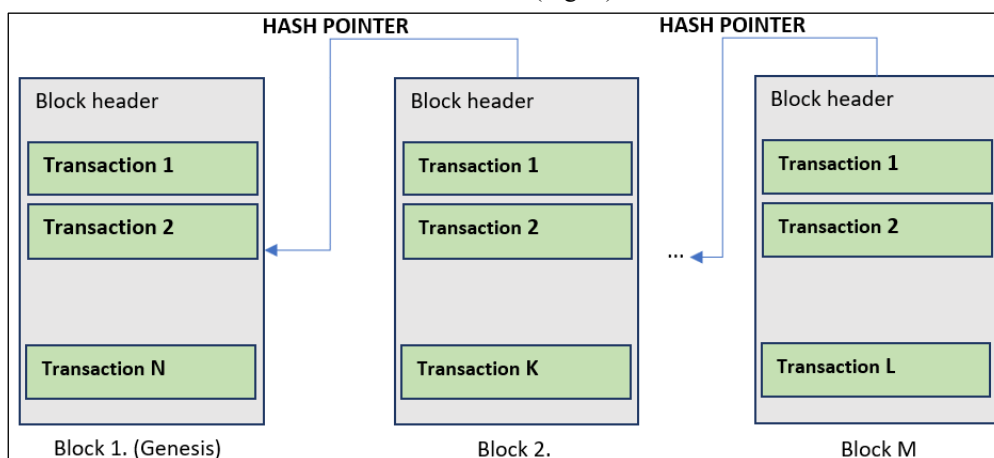

Figure 1: *Decentralized ledger*

And blockchain is the complete ledger which contains all transactions so far, all Bitcoin payments can be found in it. The essence of the proof of work algorithm is that only the user can create the commit block can authenticates the transfers, who has sufficient computing power. It is important that the more miners, the greater the competition, the more the difficulty level increases. This also means that as competition intensifies, more and more powerful devices are needed, so the electricity consumption of the Bitcoin payment network is increasing. The proof of work algorithm thus guarantees the security of the Bitcoin network, but at the same time its price is high electricity consumption, i.e. an increased ecological footprint [6]. The current energy demand of the system can also be tracked via a link: https://digiconomist.net/bitcoin-energy-consumption. It follows that with the spread of the system, the rate of electricity consumption must be solved, since it is not only Bitcoin that uses this algorithm, which can thus rival the energy consumption of the largest countries over time. In addition, due to the serious need for computing, video cards specially designed for this purpose are already being made, with high-performance chips, a process that increases the price level in the computing market, reinforces the already present chip shortage. Thus, a change in technology can also dampen this price increase.

3. PROOF OF STAKE ALGORITHM AND ITS APPLICATION

The application of the proof of work algorithm represents a step forward in the management of transactions in cryptocurrencies, ensuring that they are secure. However, due to the disadvantages mentioned above, a technological shift is required.

A solution to this can be the proof of stake algorithm, which significantly reduces power consumption. Its essence is that with its use the mining activity ceases, mining computers do not need to perform complex mathematical operations. Instead, among the miners, the system randomly selects which one can make the new block. Fraud solved with a security deposit, i.e. miners must make a deposit, and in the event of fraud, they will lose it [7].

Staking also has its drawbacks from the point of view of users. One of the biggest drawbacks of these is that the cryptocurrencies used for staking are locked for a while. Similarly to bank deposits, which cannot be accessed for a certain period of time. This may not be a problem if the value of the crypto currency rises, but there can be a serious loss if it is not possible to liquidate the stock in the event of a negative trend due to the lockdown.

In the field of cryptocurrencies, proof of stake algorithm have been used in the past, however, their capitalization is low compared to market leaders. As a novelty, in the second half of 2,022, the cryptocurrency with the second largest market capitalization, Ether (Ethereum's cryptocurrency), also switched to the system. Thus, we will present this shift below.

3.1 Ethereum

Ethereum is an open-source, public, social, blockchain-based cryptocurrency and computing platform based on distributed computing. The latter sets it apart from most cryptocurrencies, as it is also a platform that allows for solutions such as smart contract management. And with it, various applications can be built on the blockchain. The system provides a decentralized virtual computer, the Ethereum Virtual Machine (EVM), in which computational operations are performed by an international network of public nodes. The code run by the Ethereum Virtual Machine is written in the Solidity programming language. Ethereum also provides a cryptocurrency called Ether. Solidity is an object-oriented programming language that supports the development of smart contracts. The language includes the solc (Solidity Compiler) compiler, which is compatible with the Ethereum Virtual Machine and generates solidity code.

Ether is one of the most popular cryptocurrencies after the Bitcoin, which is currently the most well-known cryptocurrency. Ether Capital ranks second in the ranking of cryptocurrencies based on capitalization (Fig. 2).

#	Name	Price	Changes 24H	Changes 7D	Changes 30D	Market Cap	Volume 24H	Available Supply
☆ 1	(BTC) BITCOIN	$16,726.29	↑ 0.76%	↓ -0.69%	↓ -2.10%	$321.99 B	$12.48 B	19.25 M BTC
☆ 2	(ETH) ETHEREUM	$1,218.31	↑ 1.37%	↓ -0.08%	↓ -5.85%	$146.83 B	$3.65 B	120.53 M ETH
☆ 3	(USDT) TETHER	$1.000	↓ -0.01%	↓ -0.08%	↓ -0.05%	$66.26 B	$16.85 B	66.26 B USDT
☆ 4	(USDC) USD COIN	$1.000	↓ -0.01%	↓ -0.10%	↓ -0.10%	$44.71 B	$1.55 B	44.70 B USDC
☆ 5	(BNB) BNB	$247.07	↑ 0.72%	↑ 1.53%	↓ -15.61%	$40.35 B	$398.40 M	163.28 M BNB

Figure 2: *Order of cryptocurrencies by market capitalization (02/01/2023 www.criptofalka.hu)*

The creation of Ethereum was proposed in late 2013 by Vitalik Buterin, one of the researchers of crypto currencies. They wanted to create an altcoin that would solve the problems with Bitcoin (such as long calculated transaction times or the 51% hash rate possession problem for centralized, "miners"). The word "Altcoin" stands for "alternative coins", but it can be translated more as "alternatives to Bitcoin". All digital currencies (cryptocurrencies) built using blockchain technology are included in Bitcoin outside.

However, there is one exception in the approach of many sources: Ethereum (ETH) was the first alternative cryptocurrency to set itself a completely new goal, and to this end, its construction was very different from that of Bitcoin.

3.2 Ethereum merge

Since its launch in 2015, Ethereum has used the proof-of-work algorithm to securely add new transaction information. Mining is safe but also energy-intensive [8]. The Ethereum network as a whole, in addition to proof-of-work operation, consumes the same amount of energy per year as a smaller country, eg. Austria.

Proof-of-stake is an algorithm that consumes much less electricity. Whereas in the past, miners use high-energy computing devices, after merge, users who want to participate in the authentication of transactions put their own cryptocurrency at risk in a process called staking [9]. These approvers — also known as validators — are randomly selected to verify new information to be added to the block. They will receive an Ether reward if they participate in the validation of information. If they act unfairly, they will lose the Ether deposited. A network using a proof-of-stake mechanism works on the same principle.

Ethereum's developers expected the transition to reduce electricity consumption by as much as 0.01 TWH/yr by replacing the proof-of-work mechanism in favor of proof-of-stake corresponds to annual consumption.

There were two milestones in the preparation of the merge: the first was the creation of the Beacon Chain in December 2020 (Fig. 3). The Beacon Chain acted as a proof-of-stake network running parallel to Ethereum, where users could stake Ether. The earlier launch of the Beacon Chain was intended to have enough Ether on the network by the time of the changeover.
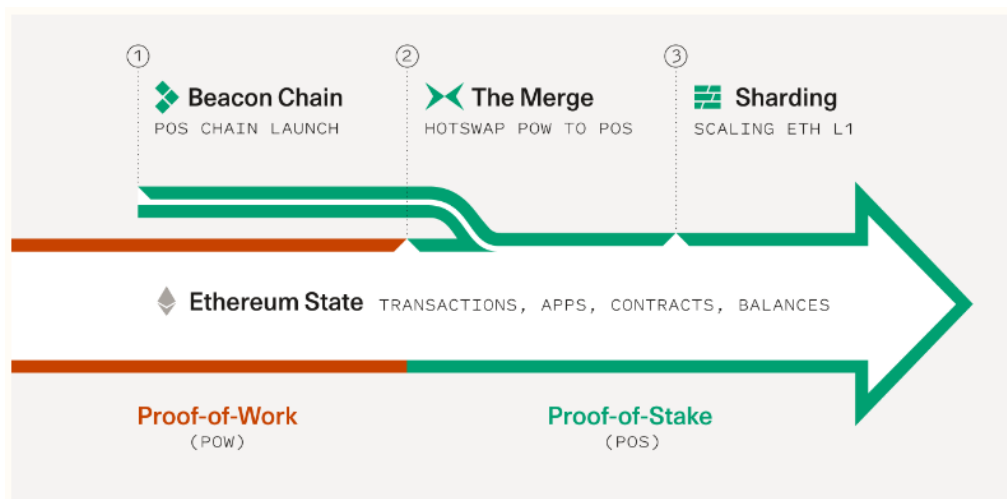
Figure 3: Ethereum Merge scheduling [10]

The Beacon Chain allowed the proof-of-stake consensus to be tested live for an extended period of time without affecting ethereum's core network, which is home to billions of dollars' worth of capital.
 As a test of Merge, Ethereum's developers performed several checks on test networks – clones of the Ethereum blockchain used for experimental purposes – during 2022.

4. RESULT

The most important result of Merge is clearly that Ethereum has become a much more environmentally friendly, secure, and future-proof platform than it has been so far (Fig. 4). This is mainly due to a drastic reduction in energy use [11]. Thanks to this, it is no longer necessary to waste significant amounts of money on electricity for mining, so fewer Ether will have to be created as a reward, such this way, the cryptocurrency can be more valuable than before.

Figure 4. Annual energy consumption (June 2022 Ethereum Foundation/ Digiconomist www.independent.co.uk/tech/ethereum-merge-crypto-energy-environment)

5. CONCLUSION

The development of Ethereum has proven how much development potential there is in blockchain technology. Its application - other than cryptocurrencies - is mostly experimental in other areas, although even the largest technology companies (e.g. IBM, Microsoft) are devoting considerable resources to the development. However, technological level jumps like merge can give a significant boost to the spread. Such developments allow other industries to access and use the technology. In the case of food chains, these advantages are also reflected, e.g. reliable data, traceable process, but several challenges still need to be solved for widespread application (e.g. return on financial investment or the attitude of the actors).

And if the databases are reliable, they can be more easily integrated into a system covering the entire process. For example, in real time, harvesters recording data during harvesting use 5G to transmit the data to a blockchain database, which is then processed by artificial intelligence. And the AI - based on the data - makes recommendations for further farming, e.g. fertilizer use, water management, etc. Thus, even the producers become interested in the use of new technologies.

6. SOURCES

[1] Sherman, A.T., Javani, F., Zhang, H., Golaszewski, E., 2019. On the Origins and Variations of Blockchain Technologies. IEEE Secur. Privacy 17, 72–77. https://doi.org/10.1109/MSEC.2019.2893730

[2] Chaum, D.L., 1979. Computer systems established, maintained, and trusted by mutually suspicious groups. Electronics Research Laboratory 11.

[3] Carrano, F.M., Sileri, P., Batt, S., Di Lorenzo, N., 2022. Blockchain in surgery: are we ready for the digital revolution? Updates Surg 74, 3–6. https://doi.org/10.1007/s13304-021-01232-y

[4] Sarmah, S.S., 2018. Understanding Blockchain Technology. Computer Science and Engineering.

[5] Yu, B., Zhan, P., Lei, M., Zhou, F., Wang, P., 2020. Food Quality Monitoring System Based on Smart Contracts and Evaluation Models. IEEE Access 8, 12479–12490. https://doi.org/10.1109/ACCESS.2020.2966020

[6] Wendl, M., Doan, M.H., Sassen, R., 2023. The environmental impact of cryptocurrencies using proof of work and proof of stake consensus algorithms: A systematic review. Journal of Environmental Management 326, 116530. https://doi.org/10.1016/j.jenvman.2022.116530

[7] Li, W., Andreina, S., Bohli, J.-M., Karame, G., 2017. Securing Proof-of-Stake Blockchain Protocols, in: Garcia-Alfaro, J., Navarro-Arribas, G., Hartenstein, H., Herrera-Joancomartí, J. (Eds.), Data Privacy Management, Cryptocurrencies and Blockchain Technology, Lecture Notes in Computer Science. Springer International Publishing, Cham, pp. 297–315. https://doi.org/10.1007/978-3-319-67816-0_17

[8] Garay, J.A., Kiayias, A., Panagiotakos, G., 2017. Proofs of Work for Blockchain Protocols Book.

[9] De Vries, A., 2023. Cryptocurrencies on the road to sustainability: Ethereum paving the way for Bitcoin. Patterns 4, 100633. https://doi.org/10.1016/j.patter.2022.100633

[10] Chen, D., 2022. Understanding the Merge [WWW Document]. Sequoia Capital US/Europe. URL https://www.sequoiacap.com/article/understanding-the-merge/ (accessed 1.3.23).

[11] Ethereum Energy Consumption, 2022. ethereum.org. URL https://ethereum.org/en/energy-consumption/ (accessed 1.2.23).

ELEMENTAL ANALYSIS OF CONTAMINATED BIOMASS ASHES FOR PHYTOMINING OF RARE EARTH ELEMENTS

[1]Truong Dinh, [1]Zsolt Dobó, [1]Helga Kovács

[1]Institute of Energy and Quality, University of Miskolc, 3515 Miskolc, Hungary
Corresponding author's email: truong.dinh@uni-miskolc.hu

ABSTRACT

Phytomining of rare earth elements (REEs) provides a potential possibility for metal recovery at brownfields where conventional mining technique is not reasonable or profitable. The holistic concept of phytomining is instituted from three scientific sectors. Phytoextraction is the first stage referred to accumulation of REEs in plants. This is followed by the enrichment process aiming to elevate metal concentration into solid remains. Eventually, extraction technology is applied to reclaim these valuable metals from the bio-ores. The main goal of this study is to identify a possible location for REEs phytomining, which lays the groundwork for further investigations. To do that, different woody biomass from disparate contaminated spots was harvested and examined. A brownfield land located in Gyöngyösoroszi, Hungary has been selected based on the elemental analysis of ash samples obtained from the incineration of the collected plants at 500 °C. The outcomes also preliminarily indicate the viability of phytomining in recovering REEs.

Keywords: brownfields, phytoextraction, rare earth metals, recovery, chemical analysis

1. INTRODUCTION

Rare earth elements (REEs) include scandium (Sc), yttrium (Y), and 15 "lanthanides" elements from lanthanum (La) to lutetium (Lu) [1]. REEs are playing an important role in green modern technologies such as hybrid cars, electric cars, wind turbines, batteries, etc [2]. These metals are also commonly used as fertilizers in agriculture to advance the quality and production of crops [3], [4]. The demand for REEs has increased remarkably causing reserve depletion, while the recycling rate reportedly is only 1% [2]. Hence, the recovery of REEs from secondary resources is a crucial issue, that has attracted a great deal of global attention in recent decades.

Phytomining is a potential manner for recycling REEs from contaminated soils where traditional mining technology is not competitive. The entire procedure of phytomining encompasses three scientific sectors; these are phytoextraction, enrichment, and extraction. At the first stage, REEs from polluted lands are accumulated in plants via phytoextraction. Two types of plants that could be efficiently used for this process are hyperaccumulators and fast-growing species [5]. In the following phase, the contaminated biomass is reduced to a manageable volume, and more importantly, these valuable metals are enriched into solid remains called bio-ores. A number of methods can be applied to achieve the enrichment purpose, which is composting, compaction, and thermal conversion (ashing, pyrolysis, gasification, combustion). Of these options, combustion is considered the most feasible and ecologically friendly manner for heightening REEs [6], [7]. Eventually, conventional or innovative extraction technologies could be utilized to extract REEs from bio-ores [8]. That is the last step to complete the phytomining route of recovering REEs from brownfield lands.

The complete approach of phytomining has been intensively investigated and widely applied to recover Nickel from polluted soils [9]–[13]. More than 500 plant species have been verified to hyper-accumulate this element [14]. The agronomic processes alongside extraction techniques have been extensively developed to produce Ni-based products such as oxide, metal, and salts [15], [16]. In another study, the whole phytomining pathway for reclaiming noble metals has been disclosed [17]. While this concept is somewhat novel in terms of REEs. The main goal of this study is to determine the possible location for the phytomining of REEs. It is

paramount as these elements are mostly dispersed in low concentrations throughout the earth's crust [18]. Identifying the viable area helps to lay the groundwork for the further steps of REEs phytomining.

2. MATERIALS AND METHODS

The resource of the contaminated biomass utilized in this research is a polluted region situated in Gyöngyösoroszi, Hungary (Mátra Mountains, Northern Hungary). In fact, it is an abandoned mining area where lead and zinc industrialized mining started in 1926 and closed in 1986 after 40 years of operation. The common plant species living there include poplar, oak, birch, pine, walnut, wattle, and bushes. Four sampling sites namely A, B, C, and D have been assigned in the abandoned mining zone, their exact locations are presented in Figure 1 and Table 1. From these places, different woody biomass comprising root and log (trunk) were collected as chemical elements are not distributed evenly in plant parts.
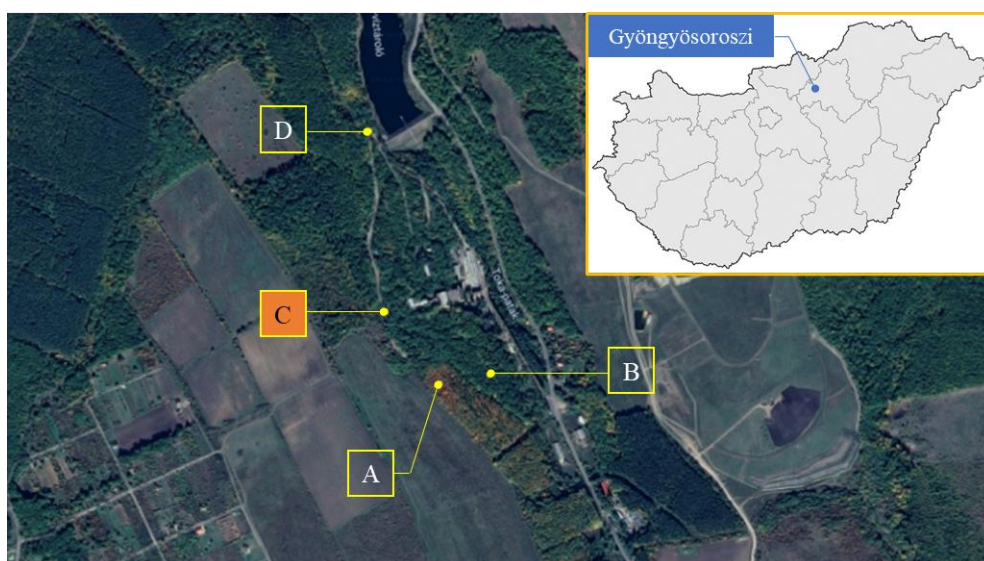

Figure 1. Sampling sites in Gyöngyösoroszi, Hungary

Table 1. The exact coordinates of the sampling sites

Sampling site	Latitude	Longitude
A	47.8420957	19.8772271
B	47.8423633	19.8785983
C	47.8434655	19.8758115
D	47.8469843	19.8752731

The harvested biomass was cleaned and rinsed in the case of root samples. Then, the biomass was left in the laboratory under natural conditions for several weeks for air drying. This was followed by drying in the oven at 105 °C for 24 hours. Afterward, the collected samples were incinerated by two-stages ashing processes. In the first step, the dried biomass was heated at 250 °C, for 2 hours with a heating rate of 50 °C/h. In the second stage, the process was carried out under the conditions as follows: heating rate 50 °C/h up to 500 °C, 4 hours waiting at 500 °C. The operation was conducted two times to secure carbon-free ash samples. The ashing temperature applied for the polluted biomass is based on previous publications [19], [20].

The chemical composition of ash samples was determined by ICP (Inductively Coupled Plasma) spectrometry, using Perkin Elmer Avio 200 inductively coupled plasma-optical emission spectrometer (ICP-OES). For the calibration of the measurement, an ICP-OES inner standard solution (Lutecium) was used. The samples were prepared based on the Hungarian standard MSZ EN 13346:2000. The analytical scale was used for taking 5 g samples for analysis. The preparation was carried out by microwave digestion with a Berghof Speedwave4 laboratory equipment, using nitric acid (2 ml, 67% concentrated) and hydrochloric acid (6 ml, 36% concentrated) solvents. The digestion and dissolution time were 30 minutes at 180 °C. The solution was filled up to 50 ml with 5% concentrated nitric acid after the filtration process using MN616 filters. The chemical measurement analyzes the concentrations of almost REEs (including Ce, Dy, Er, Eu, Gd, Ho, La, Nd, Pr, Sc, Sm, Tb, Tm, Y, Yb) in the ash samples.

3. RESULTS AND DISCUSSION

The ICP spectrometry analysis results regarding REEs concentrations in the ash samples of log and root biomass gathered from different polluted sites are shown in two tables corresponding to two metal groups. The first metal group presented in Table 2 includes Er (Erbium), Ho (Holmium), Pr (Praseodymium), Tb (Terbium), and Tm (Thulium). These elements are below the detection limit (BDL) in all the ash samples, and they are not used for further evaluations.

Table 2. Metal concentrations below the detection limit in ash samples

Element	Concentration (mg/kg)							
	Log ash				Root ash			
	A	B	C	D	A	B	C	D
Er	*<1**	*<1**	*<1**	*<1**	*<2**	*<1**	*<2**	*<1**
Ho	*<1**	*<2.5**	*<2.5**	*<2.5**	*<2.5**	*<2.5**	*<2.5**	*<1**
Pr	*<5**	*<5**	*<5**	*<5**	*<5**	*<5**	*<5**	*<5**
Tb	*<5**	*<2**	*<2**	*<2**	*<2**	*<2**	*<2**	*<5**
Tm	*<1**	*<1**	*<1**	*<1**	*<1**	*<1**	*<1**	*<1**

- A, B, C, D: sampling points
- * The concentration of the metal is BDL (below the detection limit), which is the limit that the concentration can be differentiated from the background noise.

The second metal group consists of Ce (Cerium), Dy (Dysprosium), Eu (Europium), Gd (Gadolinium), La (Lanthanum), Nd (Neodymium), Sc (Scandium), Sm (Samarium), Y (Yttrium) and Yb (Ytterbium); which are observed in at least one sample. They are given in Table 3 and are used for further investigations. The concentration magnitudes were colorized in the increasing order of green-yellow-red (Table 3). Besides that, the measurement results were also visualized into graphs shown in Figure 2.

Table 3. The concentration of detectable REEs in ash samples of biomass gathered from different contaminated sites

Element	Concentration (mg/kg)							
	Log ash				Root ash			
	A	B	C	D	A	B	C	D
Ce	*<1**	*<2**	3.12	3.72	41.69	7.14	29.49	17.81
Dy	*<2**	*<2**	*<2**	*<2**	3.20	*<2**	*<2**	*<2**

Element	Concentration (mg/kg)							
	Log ash				Root ash			
	A	B	C	D	A	B	C	D
Eu	<0.5*	<0.5*	<0.5*	<0.5*	0.67	<0.5*	0.78	<0.5*
Gd	<1*	2.55	2.52	1.68	9.93	3.38	6.60	<2*
La	1.43	0.75	2.20	2.43	23.68	4.52	13.45	10.90
Nd	<1*	<1*	<1*	<1*	18.13	<5*	14.70	6.30
Sc	<0.5*	<0.5*	<0.5*	<0.5*	7.23	1.86	7.75	3.82
Sm	<1*	<1*	<1*	<1*	5.56	<2*	4.73	2.53
Y	0.64	<0.5*	0.77	1.30	17.79	5.61	10.47	10.13
Yb	<2.5*	<0.5*	<0.5*	<0.5*	1.81	<0.5*	1.02	<2.5*

- A, B, C, D: sampling points
- * The concentration of the metal is BDL (below the detection limit), which is the limit that the concentration can be differentiated from the background noise.
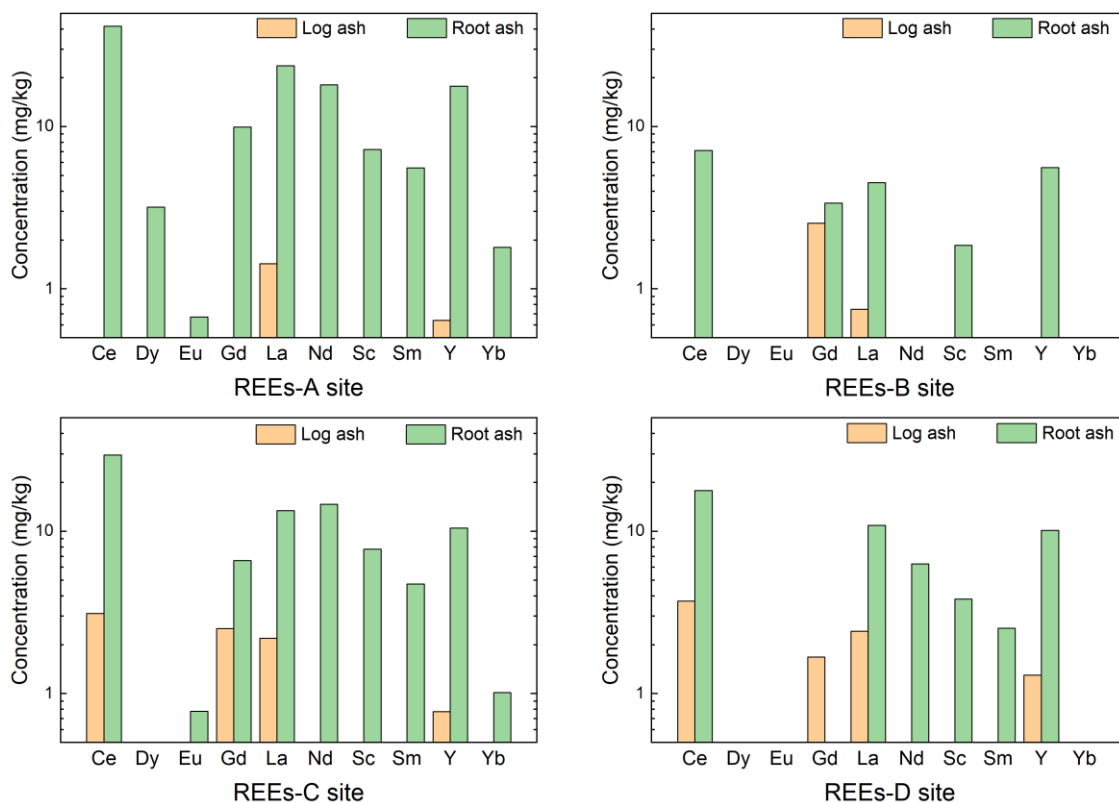

Figure 2. The concentration of REEs in the log and root ash samples of biomass gathered from different contaminated sites

In terms of log ash and root ash together, REEs were most identified in the samples collected from the C site (Figure 2). To be specific, four elements comprising Ce, Gd, La, and Y were found in both log and root ash

samples, and five more REEs (Eu, Nd, Sc, Sm, Yb) were detected in root ash of biomass coming from this area. The concentration of REEs in the solid remains obtained from polluted site C is quite high compared to that in other sampling points. Because of the mentioned reasons, site C has been selected as the attainable location for further investigations of REEs phytomining.

REEs were considerably detectable, ten of those elements were determined in the ash of biomass gathered from the brownfields. Their concentrations are in a wide range from less than one to dozens of ppm. The elements such as Europium and Ytterbium were barely found, while Cerium, Lanthanum, and Samarium showed the highest concentrations of 41.69, 23.68, and 18.13 mg/kg respectively in the ash of biomass harvested from location A. In terms of total rare earth minerals, the levels are as high as 130 and 89 mg/kg observed in root ashes of the A and C sites. These numbers are relatively high, so extraction of REEs from ashes coming from contaminated biomass has great potential.

The graphs in Figure 2 also present the distribution of REEs. It indicates that the concentration of REEs in the root ash is higher than in the log ash. The results are in good agreement with other studies [21]–[23]. That can be explained by the distribution of metals in the below-ground part (root). It is usually higher than in log [24], [25] but other above-ground parts (foliage, leaves, etc.) could also accumulate higher concentrations of them [22], [26].

4. CONCLUSIONS

In the spirit of specifying an attainable location for REEs phytomining, different types of woody biomass encompassing root and log were collected from four metal-polluted sites located in Gy ngy soroszi, Hungary. The harvested plants were incinerated at 500 °C to generate ashes for ICP analysis. According to the elemental analytical outcomes, the contaminated spot C has been chosen for further research of REEs phytomining due to the following reasons. In terms of log ash and root ash together, REEs were most detected in the samples gathered from there. The concentrations of the detectable metals in the solid residuals from site C are relatively high compared to other sampling points. The chemical measurements also indicate that the concentration of REEs in the root ash is higher than that in the log ash, which is an essential input for further investigations. It is worth noting that the concentration of REEs is significant in bio-ores obtained from contaminated biomass, and the solid remains are promising metal resources. In the following work, the plants coming from selected location C would be combusted. Solid residues such as bottom ash, fly ash, and deposited ash from several positions in the combustion and flue gas system will be captured and analyzed. Further directions would be defined on the basis of the chemical analysis results.

REFERENCES

[1]   D. Schüler, M. Buchert, R. Liu, S. Dittrich, and C. Merz, "Study on rare earths and their recycling," *Öko-Institut eV Darmstadt*, vol. 49, pp. 30–40, 2011.

[2]   V. Balaram, "Rare earth elements: A review of applications, occurrence, exploration, analysis, recycling, and environmental impact," *Geosci. Front.*, vol. 10, no. 4, pp. 1285–1303, Jul. 2019,

doi: 10.1016/j.gsf.2018.12.005.

[3]   X. Pang, D. Li, and A. Peng, "Application of rare-earth elements in the agriculture of china and its environmental behavior in soil," *J. Soils Sediments*, vol. 1, no. 2, pp. 124–129, Jun. 2001, doi: 10.1007/BF02987718.

[4]   K. Redling, "Rare earth elements in agriculture with emphasis on animal husbandry." lmu, 2006.

[5]   A. van der Ent, A. J. M. Baker, R. D. Reeves, A. J. Pollard, and H. Schat, "Hyperaccumulators of metal and metalloid trace elements: Facts and fiction," *Plant Soil*, vol. 362, no. 1–2, pp. 319–334, 2013, doi: 10.1007/s11104-012-1287-3.

[6]   A. Sas-Nowosielska, R. Kucharski, E. Małkowski, M. Pogrzeba, J. M. Kuperberg, and K. Kryński, "Phytoextraction crop disposal - An unsolved problem," *Environ. Pollut.*, vol. 128, no. 3, pp. 373–379, 2004, doi: 10.1016/j.envpol.2003.09.012.

[7]   H. Kovacs and K. Szemmelveisz, "Disposal options for polluted plants grown on heavy metal contaminated brownfield lands – A review," *Chemosphere*, vol. 166, pp. 8–20, 2017, doi: 10.1016/j.chemosphere.2016.09.076.

[8]   M. Wang, Q. Tan, J. F. Chiang, and J. Li, "Recovery of rare and precious metals from urban mines—A review," *Front. Environ. Sci. Eng.*, vol. 11, no. 5, pp. 1–17, 2017, doi: 10.1007/s11783-017-0963-1.

[9]   B. Jally, B. Laubie, Y.-T. Tang, and M.-O. Simonnot, "Processing of Plants to Products: Gold, REEs and Other Elements," 2021, pp. 63–74. doi: 10.1007/978-3-030-58904-2_4.

[10]   R. L. Chaney, "Phytoextraction and phytomining of soil nickel," in *Nickel in Soils and Plants*, CRC Press, 2018, pp. 341–374.

[11]   X. Zhang, V. Houzelot, A. Bani, J. L. Morel, G. Echevarria, and M.-O. Simonnot, "Selection and Combustion of Ni-Hyperaccumulators for the Phytomining Process," *Int. J. Phytoremediation*, vol. 16, no. 10, pp. 1058–1072, Oct. 2014, doi: 10.1080/15226514.2013.810585.

[12]   B. Laubie, J. Vaughan, and M.-O. Simonnot, "Processing of Hyperaccumulator Plants to Nickel Products BT - Agromining: Farming for Metals: Extracting Unconventional Resources Using Plants," A. van der Ent, A. J. M. Baker, G. Echevarria, M.-O. Simonnot, and J. L. Morel, Eds. Cham: Springer International Publishing, 2021, pp. 47–61. doi: 10.1007/978-3-030-58904-2_3.

[13]   A. Tognacchini *et al.*, "Agromining from Secondary Resources: Recovery of Nickel and Other Valuable Elements from Waste Materials BT - Agromining: Farming for Metals: Extracting Unconventional Resources Using Plants," A. van der Ent, A. J. M. Baker, G. Echevarria, M.-O. Simonnot, and J. L. Morel, Eds. Cham: Springer International Publishing, 2021, pp. 299–321. doi: 10.1007/978-3-030-58904-2_14.

[14]   R. D. Reeves, A. J. M. Baker, T. Jaffré, P. D. Erskine, G. Echevarria, and A. Ent, "A global database for plants that hyperaccumulate metal and metalloid trace elements," *New Phytol.*, vol. 218, no. 2, pp. 407–411, Apr. 2018, doi: 10.1111/nph.14907.

[15]   A. Bani, G. Echevarria, S. Sulçe, and J. L. Morel, "Improving the Agronomy of Alyssum murale for Extensive Phytomining: A Five-Year Field Study," *Int. J. Phytoremediation*, vol. 17, no. 2, pp. 117–127, Feb. 2015, doi: 10.1080/15226514.2013.862204.

[16]   X. Zhang, B. Laubie, V. Houzelot, E. Plasari, G. Echevarria, and M.-O. Simonnot, "Increasing purity of ammonium nickel sulfate hexahydrate and production sustainability in a nickel phytomining process," *Chem. Eng. Res. Des.*, vol. 106, pp. 26–32, Feb. 2016, doi: 10.1016/j.cherd.2015.12.009.

[17]   T. Dinh, Z. Dobo, and H. Kovacs, "Phytomining of noble metals – A review," *Chemosphere*, vol. 286, p. 131805, Jan. 2022, doi: 10.1016/j.chemosphere.2021.131805.

[18]   W. M. Haynes, *CRC Handbook of Chemistry and Physics*. CRC Press, 2016. [Online]. Available: https://books.google.hu/books?id=VVezDAAAQBAJ

[19]   B. D. Krisnayanti, C. W. N. Anderson, S. Sukartono, Y. Afandi, H. Suheri, and A. Ekawanti, "Phytomining for artisanal gold mine tailings management," *Minerals*, vol. 6, no. 3, pp. 1–11,

2016, doi: 10.3390/min6030084.

[20] A. E. Lamb, C. W. N. Anderson, and R. G. Haverkamp, "The extraction of gold from plants and its application to phytomining," 2001.

[21] M. Yuan *et al.*, "Accumulation and fractionation of rare earth elements (REEs) in the naturally grown Phytolacca americana L. in southern China," *Int. J. Phytoremediation*, vol. 20, no. 5, pp. 415–423, Apr. 2018, doi: 10.1080/15226514.2017.1365336.

[22] W. Zhenggui *et al.*, "Rare earth elements in naturally grown fern Dicranopteris linearis in relation to their variation in soils in South-Jiangxi region (Southern China)," *Environ. Pollut.*, vol. 114, no. 3, pp. 345–355, 2001, doi: 10.1016/S0269-7491(00)00240-2.

[23] L. Miao, Y. Ma, R. Xu, and W. Yan, "Environmental biogeochemical characteristics of rare earth elements in soil and soil-grown plants of the Hetai goldfield, Guangdong Province, China," *Environ. Earth Sci.*, vol. 63, no. 3, pp. 501–511, 2011, doi: 10.1007/s12665-010-0718-9.

[24] X. Xu, W. Zhu, Z. Wang, and G. J. Witkamp, "Distributions of rare earths and heavy metals in field-grown maize after application of rare earth-containing fertilizer," *Sci. Total Environ.*, vol. 293, no. 1–3, pp. 97–105, 2002, doi: 10.1016/S0048-9697(01)01150-0.

[25] H. Kovacs, O. Bánhidi, and K. Veisz, "Distribution of chemical elements within ligneous parts of various trees," *Mater Sci Eng*, vol. 36, pp. 41–50, Jan. 2011.

[26] S. M. Ding, T. Liang, J. C. Yan, Z. L. Zhang, Z. C. Huang, and Y. N. Xie, "Fractionations of rare earth elements in plants and their conceptive model," *Sci. China, Ser. C Life Sci.*, vol. 50, no. 1, pp. 47–55, 2007, doi: 10.1007/s11427-007-2040-7.

EXAMINATION OF THE COMPOSITION AND DIELECTRIC PROPERTIES OF WINES FROM THE CSONGRÁD WINE REGION

[1]Blanka Juhász, [2]Zoltán Péter Jákói [1]Balázs Lemmer

[1]University of Szeged, Faculty of Engineering, Department of Food Engineering,
Moszkvai krt. 5-7., H-6725, Szeged, Hungary
[2]University of Szeged, Faculty of Engineering, Department of Biosystems Engineering,
Moszkvai krt. 5-7., H-6725, Szeged, Hungary

e-mail: lemmer@mk.u-szeged.hu,,

ABSTRACT

In Hungary, viticulture and winemaking have a very long tradition and culture. Nowadays, more and more consumers are paying attention to the nutritional properties of the food they consume, in addition to their enjoyment value. Wines can have an outstanding antioxidant content. The amount of antioxidants can be influenced by a number of parameters (wine-making technology, grape variety, area under vines, etc.). Antioxidants play an important role in the preservation of health, as well as inhibiting oxidation processes in food. Dielectric material analysis methods are also increasingly used in the food industry. The great advantages of dielectric testing include its chemical-free nature and the speed of the test. In our studies, we have investigated the food properties, i.e. alcohol, acid and antioxidant content and dielectric properties of different wine samples.

Keywords: wine, dielectric, antioxidant

1. INTRODUCTION

Science has long been interested in the physiological effects of wine beyond its pleasure value. Among the physiological properties, antioxidant compounds have been recognised for a long time. Such compounds are found in higher amounts in red wines than in white wines, but white wines also have such compounds. The source of antioxidants in wine comes primarily from the grapes used as the raw material. Scientific research on bioactive compounds has shown the effects of plant-based diets on cardiovascular disease (CVD) and cancer. Scientific research in the field of disease prevention has shown that plant-based foods contain a number of components that effectively enhance the antioxidant defence potential of the human body [1].

A number of different biologically active substances, phytochemicals, are found in plants and have positive physiological and pharmacological effects. They are divided into different groups based on their chemical structure and functional properties. The main groups are: carotenoids, phytosterols, glucosinolates, flavonoids, phenolic acids, protein inhibitors, monoterpenes, phytoestrogens, sulphur compounds. These compounds vary widely in chemical structure and function [2]. Only the groups of compounds that are also found in grapes will be discussed below.

In the case of grapes and wine, mention should be made of phenolic compounds, which have also been studied in cereals, pulses, nuts, olive oil, vegetables, fruits and teas, in addition to grapes and wine [3]. They have a much wider spectrum of activity than other bioactive compounds [4]. Some studies show that flavonoids have beneficial effects on thrombosis and tumourigenesis. Some flavonoids have antioxidant effects, inhibit atherosclerosis and the development of [5]. Various phytoestrogens are present in soy, but also in linseed oil, whole grains, fruits and vegetables and grapes as well. They bind to the same receptors as endogenous oestrogens, but their hormonal effects are significantly smaller. They can positively influence carcinogenesis, cardiovascular disease and osteoporosis. Isoflavonoids are effective in the prevention of viral diseases. Sulphides such as allium compounds have anticarcinogenic, antioxidant and anti-inflammatory effects. Coumarins inhibit blood clotting, inflammatory processes and the development of [6]. In summary, many bioactive compounds of plant origin have beneficial effects on our body and their role in preventive

action is undisputed, although their mechanism of action is not fully understood. There is sufficient evidence to recommend the consumption of foods rich in bioactive compounds. In practical terms this means that a diet rich in a variety of fruits, vegetables, whole grains, pulses, oils and nuts is recommended [1]

The main components of wine, apart from water, are alcohols (mainly ethanol) and acids. These components have a significant influence on the organoleptic properties [7], and some of them also have the antioxidant properties discussed above. Among the acids, tartaric acid is the most important, but there are also a number of other carboxylic acids and sulphuric acid used in wine-making technology. There are many methods for the detection of alcohol and acids, and in Hungary and in many other countries, including the EU, standards have been set out as officially accepted procedures [8,9].

Quick methods that do not require large amounts of chemicals are becoming increasingly important in the testing of various materials, including foodstuffs. Such techniques include various dielectric measurement methods [10,11].

The dielectric behaviour of different materials, i.e. the interaction between the electromagnetic field and the material, is defined by their electrodynamic properties and influenced by several factors. These factors include, for example, the physical and chemical properties, structure and temperature of the material, but also the frequency (ω) and field strength (E) of the applied electromagnetic field [12-14].

The absolute permittivity of a material is a constant (ε) characteristic of a material quality, which is the ratio of the electromagnetic field strength (E) to the electric displacement (D). The absolute permittivity (ε) includes all the characteristics that determine the adsorption of electric/electromagnetic energy within the material and the energy loss that occurs after the electromagnetic wave is absorbed within the material. The dielectric constant ε' represents the electrical energy storage capacity of the material, while ε'' represents the total dielectric loss and shows how much of the stored electrical energy is transformed into other forms of energy (e.g. heat or kinetic energy) [15].

The aim of our work was to search for relationships between the properties described above, i.e. antioxidant, acid and alcohol content, and dielectric properties. We have also investigated the differences between wines made from similar grape type harvested in the same field.

2. MATERIALS AND METHODS

2.1. Wine samples

Our wine samples are obtained from a producer in the Csongrád wine region. Three white wine samples and one red wine sample were used in our tests. The grapes for the Riesling white wines were from the same area, with vintage and technique (oxidative/reductive) differences. Table 1. represents the samples of our study. The wines were filled into 0.5 litre PET bottles at the time of purchase and kept at 4 °C until the tests.

Table 1. Wine types of the study

Wine type	Vintage	Technique	Nomination
Rhine Riesling	2021	oxidative	A
Rhine Riesling	2021	reductive	B
Rhine Riesling	2022	reductive	C
Blue Franc	2021	oxidative	D

2.2 Dielectric properties

Dielectric properties i.e., dielectric constant (ε') and dielectric loss factor (ε'') was measured by a Dielectric Assessment Kit (SPEAG, Switzerland) (Fig. 1.). The kit used in this study contains an open-ended coaxial dielectric probe (DAK 3.5), connected to a vector network analyser (ZVL-3, Rhode&Swarz, Germany). Dielectric measurements were carried out in the frequency range of 200MHz-2.4GHz at constant temperature of 20°C. The data from the network analyser was processed by specific computer software of DAK and exported to MS Excel for further study. Every date presented in this study is the average value of 30 sequential measurements.
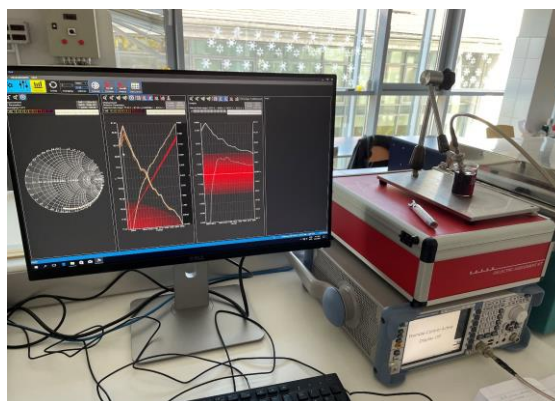

Figure 1. The DAK measuring system and the specific DAK software

2.3. Alcohol and acid content

The alcohol content was determined according to MSZ 9458 standard [8]. $100cm^3$ of wine sample was poured into a round-bottomed flask and distilled to produce 75-80 cm^3 of distillate (fig 2.). The distillate was made up to $100cm^3$ with distilled water and the relative density of the diluted distillate was determined at the temperature of 20°C using a pycnometer. Knowing the relative density, the alcohol content can be determined from a table. results are expressed as a percentage by volume.

Figure 2. Alcohol content determination

The determination of the acidity was also carried out using a standard method (MSZ 9472) [9]. A 0.1 M solution of Na hydroxide was used to titrate the wine sample to neutral (7.0) pH using a pH meter. The carbon dioxide content was removed from the wine before the measurement. After titration, the acidity was determined using Eq. 1.

$$A = \frac{V_{NaOH} \cdot f}{V_w} \tag{1}$$

Where A is the acidity of the sample in tartaric acid equivalent [gL^{-1}], V_{NaOH} is the rate of consumption of a 0,1M NaOH solution [cm^3], f is the acidity corresponding to the consumption of 1 cm^3 of the measuring solution [gL^{-1}] and Vw is the volume of the volume of the titrated wine sample [cm^3].

The free radical scavenging activity of the wines was determined using the DPPH (1,1-diphenyl-2-picrylhydrazyl) method. During the reaction, the dark purple stable radical loses its colour when reacting with antioxidants. This method is quick, the measurement is simple, and the radical is commercially available. Its disadvantage is that it uses a stable radical, which does not occur in living organisms, so it is not possible to determine accurately how reactive the antioxidants in the sample are to biological radicals [16]. It is light, oxygen, pH, temperature, and solvent dependent [17].
As a first step, a stock solution was prepared using 39.5mg DPPH reagent and 10cm^3 of 96% ethanol. After complete dissolution, a working solution was prepared by diluting 500cm^3 of 96% ethanol to a final volume of 5cm^3 of stock solution with 96% ethanol. A mixture of 1cm^3 of 96% ethanol and 6cm3 of working solution was used as a control sample, while for the wine samples 1-1cm^3 of wine was pipetted instead of ethanol. After thorough mixing, the samples were kept in the dark for 30min and their absorbance was measured at 517 nm. The calculation of the antioxidant capacity according to DPPH method is presented in Eq 2.

$$DPPH = \frac{A_0 - A_w}{A_0} \cdot 100\% \tag{2}$$

Where A_0 is the absorbance of the control sample [-] and A_s is the absorbance of wine samples [-].

3. RESULTS AND DISCUSSION

The aim of our work was to look for a correlation between the different food properties of wines and their dielectric properties, and to investigate the differences between wines from the same place, from different vintages and produced using different techniques.

3.1. Antioxidant capacity

First, the antioxidant content of the wines was analysed using the DPPH method. During the tests, 5 parallel measurements were performed, the average of which is shown in Fig 3.
The red wine included in the study is not presented in the figure, as this wine (unsurprisingly) had a significantly higher antioxidant content (15.46%) than the white wine. Among the Rhine Rieslings, the highest values were obtained for the 2021 vintage sample (B), which was prepared using the reductive method (1.4%). Lower values were obtained, but not significantly different from this (1.23%), taking into account the standard deviation.
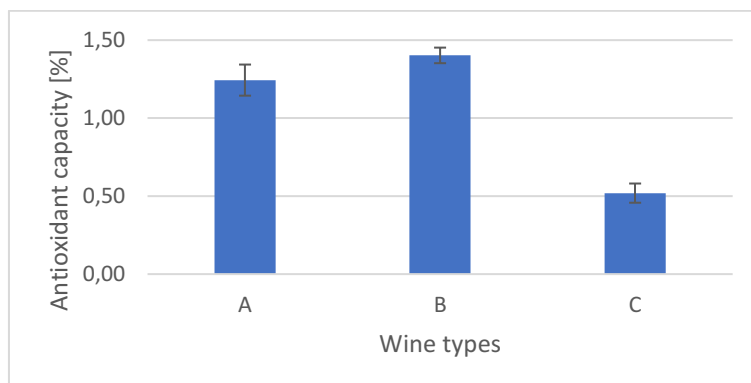
Figure 3. Antioxidant capacity of different Rhone Riesling samples

The 2021 samples contained significantly fewer compounds with antioxidant activity than the 2022 wine (C). Here, the antioxidant capacity was less than half (0.52%) of the previous values. These results suggest that the vintage of the wine, i.e. presumably the composition of the raw material, has a greater influence on the antioxidant activity of the wine than the winemaking technique.

3.2. Alcohol content and acidity

The alcohol content of the wines was examined next. Our results are presented in Fig. 4. The values were between 10,7 and 12,6. The lowest value was obtained in the case of Blue Franc D, with an alcohol content of 10.7%. This is considered significant when the standard deviation is taken into account.
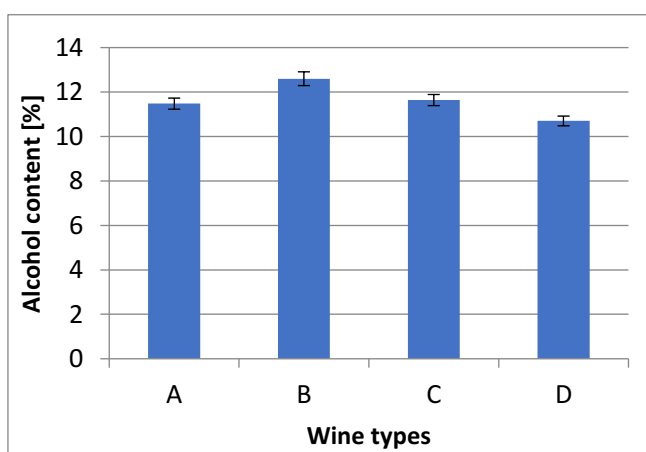

Figure 4. Alcohol content of the wine samples

Among the white wines, the wines labelled A and C did not differ significantly, with alcohol contents of 11.48 and 11.64% respectively. This result can be considered significant in that neither the vintage nor the technique were identical. A significantly higher value than the others was obtained with the 2021 reductive Rhine Riesling marked B.

As far as acidity is concerned, the values for each wine are significantly different from all the others (Fig. 5.). The lowest value was observed for red wine D. For the differences in oxidative (A) and reductive (B) techniques only, there was a very significant difference of 1.6 times for the same vintage. The oxidative wine had an acidity of almost 7 gL^{-1}, while the reductive wine had an acidity of only 4.3 gL^{-1}. When the two reductive Rhine Rieslings are compared, it can be seen that the vintage also has a significant influence on acidity. The 2022 wine was nearly 1.4 times higher than the 2021 wine, with a value of 5.8 g^{L-1}.
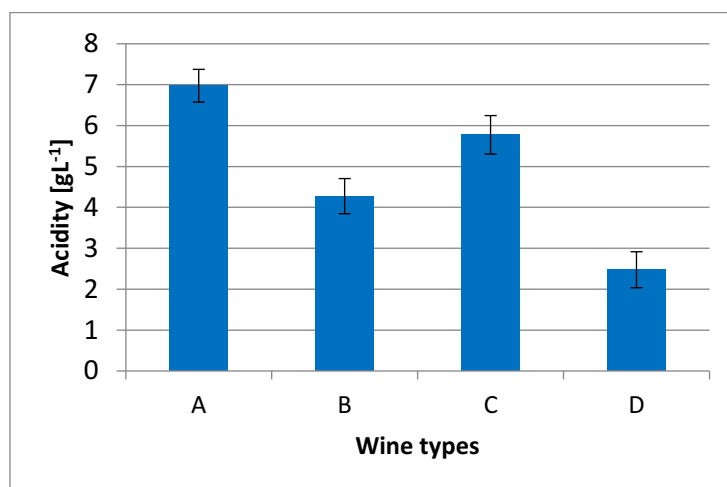

Figure 5. Acidity of the wine samples

3.3. Dielectric properties

Regarding the evolution of the dielectric constant (ε') on Fig. 6, it can be said that a difference is observed at lower frequency values for the different wines. Above 600 MHz the differences start to disappear considerably, and above 1000 MHz there is practically no difference between the dielectric constants of the different samples.
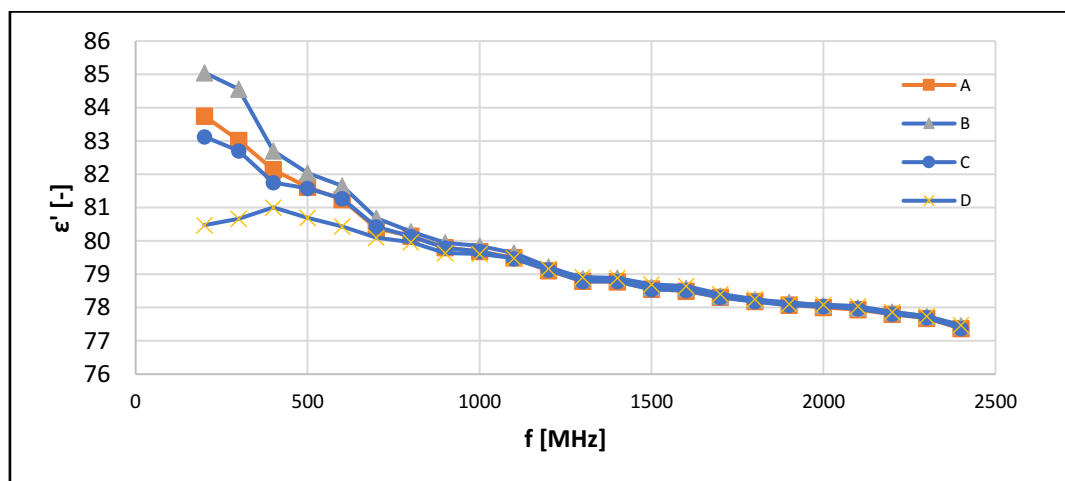

Figure 6. Dielectric constant (ε') in the function of frequency (f)

In most cases, the values decrease with increasing frequency. The only sample with a different trend is sample D (blue franc): between 200 and 400 MHz the dielectric constant increases and only starts to decrease at higher frequency values. As long as there are noticeable differences between the different wines, it can be said that white wines have a higher dielectric constant. The oxidative Rhine Riesling of 2021 marked A is steady, whereas for the reductive wines a break is seen when the measurement frequency is increased from 300 to 400 MHz. Our results suggest that the dielectric constant value measured at the lower frequency (200-600 MHz) can be used to infer the winemaking technique.

For the loss factor (ε''), an increasing trend is observed for all wine types at increasing measurement frequency (Fig. 7). Primary differences are also observed at lower frequencies, as for the dielectric constant. The values for white wine (A) produced by the oxidative technique start to increase already at low frequencies, whereas for the reductive ones this increase is only observed later. In the case of red wine (D), this increase starts at even higher frequencies, and it can also be said that the ε'' values for this wine are lower, with the difference becoming narrower at higher frequencies. Similar to what was described for the dielectric constant, it can be said that wine making techniques can be concluded from the dielectric loss factor values.
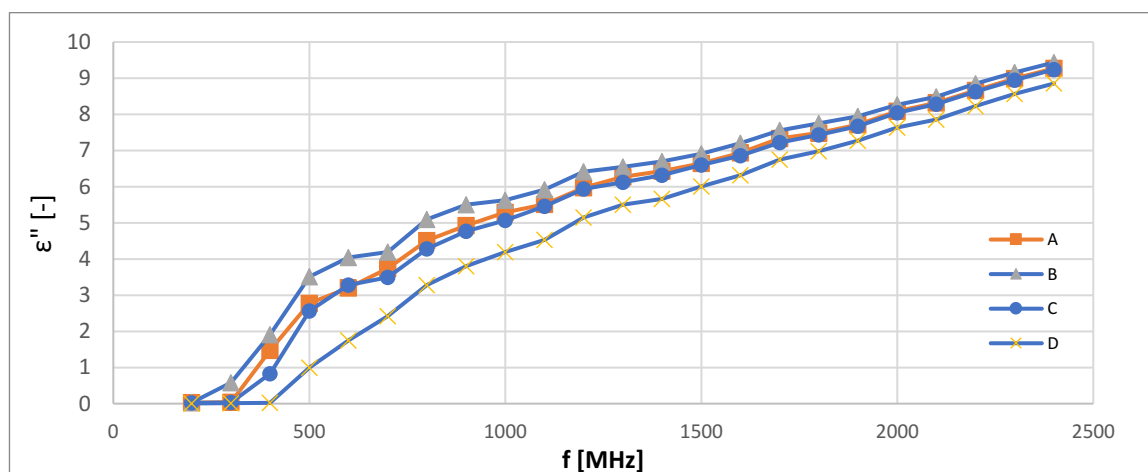

Figure 7. Dielectric loss factor (ε'') in the function of frequency (f)

4. CONCLUSIONS

In the present study, four different wines, a Blue Franc and three Rhone Rieslings, were analysed. The Rieslings were from two vintages, both oxidative and reductive, and the grapes were from the same area. The antioxidant activity, alcohol content, acidity and dielectric properties of the wines were analysed.

Our results showed that, even for the same variety, winemaking technique and growing area, differences between wines can be detected. In terms of free radical scavenging capacity, the influence of the ageing process is greater. For acidity, the oxidative or reductive nature of the wine and the vintage were found to have a strong influence on acidity.

For the dielectric parameters, i.e. dielectric constant and loss factor, it was also found that wine shows more significant differences at lower frequencies. The slope of the dielectric constant curves as a function of the measurement frequency was similar for white wines produced by the reductive method, and thus the method of vinification can be interpreted. Differences were also visible in the dielectric loss factor, with the main differences being found at the critical measurement frequency where the loss factor values increased.

Our results suggest that the determination of dielectric properties may be a useful tool to determine the differences between wines, and it may be worth extending the tests to more wine samples,

REFERENCES

[1] Kris-Etherton, Penny M. Hecker, Kari D. Bonanome, Andrea Coval, Stacie M. Binkoski, Amy E. Hilpert, Kirsten F. Griel, Amy E. Etherton, Terry D.: Bioactive compounds in foods; their role in the preventation of cardiovascular disease and cancer American Journal of Medicine. Dec 30, 2002, Vol. 113 Issue 9B, S,

[2] Santos-Sánchez, N. F., Salas-Coronado, R., Villanueva-Cañongo, C., & Hernández-Carlos, B. (2019). Antioxidant compounds and their antioxidant mechanism. Antioxidants, 10, 1-29.

[3] Garrido, J., & Borges, F. (2013). Wine and grape polyphenols—A chemical perspective. Food research international, 54(2), 1844-1858.

[4] Gutiérrez-Escobar, R., Aliaño-González, M. J., & Cantos-Villar, E. (2021). Wine polyphenol content and its influence on wine quality and properties: A review. Molecules, 26(3), 718.

[5] Gutiérrez-Escobar, R., Aliaño-González, M. J., & Cantos-Villar, E. (2021). Wine polyphenol content and its influence on wine quality and properties: A review. Molecules, 26(3), 718.

[6] Lacy, A., & O'Kennedy, R. (2004). Studies on coumarins and coumarin-related compounds to determine their therapeutic role in the treatment of cancer. Current pharmaceutical design, 10(30), 3797-3811.

[7] Jordão, A. M., Vilela, A., & Cosme, F. (2015). From sugar of grape to alcohol of wine: Sensorial impact of alcohol in wine. Beverages, 1(4), 292-310.

[8] MSZ 9458 Wine analysis, determination of alcohol content by distilling method; Hungarian Standard

[9] MSZ 9472 Determination of the total acidity of wines; Hungarian Standard

[10] Dobozi, R., Jákói, Z. P., Csanádi, J., & Beszédes, S. (2023). Investigating the Acid-and Enzyme-Induced Coagulation of Raw Milk Using Dielectric and Rheological Measurements. Applied Sciences, 13(10), 6185.

[11] Kovács, P. V., Lemmer, B., Keszthelyi-Szabó, G., Hodúr, C., & Beszédes, S. (2018). Application of dielectric constant measurement in microwave sludge disintegration and wastewater purification processes. Water Science and Technology, 77(9), 2284-2291.

[12] Géczi, G., & Sembery, P. (2005). Mikrohullám az élelmiszeriparban. Áram és technológia, 3, 19-21.

[13] Sembery, P., & Géczi, G. (2008). Microwave treatment of food. Hungarian Agricultural Research, 17(2-3), 12-16.

[14] Appleton, T. J., Colder, R. I., Kingman, S. W., Lowndes, I. S., & Read, A. G. (2005). Microwave technology for energy-efficient processing of waste. Applied energy, 81(1), 85-113.

[15] Kumar, A., Sharma, S., & Singh, G. (2007). Measurement of dielectric constant and loss factor of the dielectric material at microwave frequencies. Progress In Electromagnetics Research, 69, 47-54.

[16] Frankel, E. N., & Meyer, A. S. (2000). The problems of using one-dimensional methods to evaluate multifunctional food and biological antioxidants. Journal of the Science of Food and Agriculture, 80(13), 1925-1941.

[17] Prior, R. L., & Cao, G. (1999). In vivo total antioxidant capacity: comparison of different analytical methods1. Free radical biology and medicine, 27(11-12), 1173-1181.

MONITORING THE PROCESS OF YOGURT SPOILAGE BY DIELECTRIC MEASUREMENTS AND SPREAD PLATE METHOD

[1]Réka Dobozi

[1]University of Szeged, Faculty of Engineering, Department of Food Engineering, H-6725 Szeged, Mars tér 7.

ABSTRACT

In my research work, I primarily focused on the investigation of yogurt (made from home-made raw milk) spoilage by microbiological and dielectric measurements. During the experiment, I continuously monitored the changes in aerobic and anaerobic *Lactobacillus* cell counts of the product, as a possible spoilage process would cause the deteriorative microbes to displace the lactic acid bacteria, and I also monitored the changes in the dielectric properties of the sample material at 400 MHz frequency. The research results verified that there is a strong correlation between the variation in live cell counts and dielectric parameters in both aerobically and anaerobically cultured lactic acid bacteria. The main conclusions of the results are that the change in the bacterial count, and thus the deterioration process leading to it, can be indirectly monitored in the dairy product under study by low-frequency determination of both the dielectric constant and the loss factor.

Keywords: yogurt spoilage, dielectric measurements, microbiological properties

1. INTRODUCTION

Yogurt is a popular fermented dairy product enjoyed by many individuals around the world due to its nutritional value and taste. However, yogurt spoilage is a common problem that affects its quality, safety, and shelf life. Spoilage of yogurt can occur due to a variety of factors such as contamination with undesirable microorganisms, pH changes, and temperature abuse during storage and distribution. Yogurt contains lactic acid bacteria, which play a critical role in the fermentation process, which results in the characteristic texture, flavor, and aroma of yogurt. However, the microbiological stability of yogurt is vulnerable to various factors that can lead to spoilage. Microbial spoilage of yogurt is a significant concern for the dairy industry, as it can result in changes in product quality, sensory attributes, and safety. Understanding the microbiological aspects of yogurt spoilage is crucial for developing effective strategies to prevent or control spoilage and ensure the shelf-life of the product [1].

The electric field strength (E, unit: Vm^{-1}) is a vector of fields characterising the electric or electromagnetic field at each point in the field and showing the extent to which the electric/electromagnetic field exerts a force on the material that is in contact with it. In a time-invariant (static) electromagnetic field with a point charge of Q, the electric field strength can be written as:

$$E(r) = \frac{1}{4\pi \cdot \varepsilon} \cdot \frac{Q}{|r|^3} \cdot r \tag{1}$$

In the equation, r is the vector from the point charge to the point of measurement and ε is the absolute dielectric permittivity of the material under test at that point. If there are n number of point charges in the field, the resultant field strength can be calculated from the superposition of the field generated by the point charges. For time-varying, i.e. dynamic electromagnetic fields, the field strength can be given by Maxwell's equations. When a material interacts with an electric or electromagnetic field E, it can cause a charge movement or dipole rearrangement in the material, depending on its composition and structure. The extent of this is characterised by the so-called electric (dielectric) shift (D), which is a vector quantity, i.e. it has

magnitude and direction. The relationship between the electric field strength and the electric shift is given by the absolute permittivity (ε) of the materials:

$$\varepsilon = \frac{D}{E}; \; \left[\frac{As}{Vm}\right] \tag{2}$$

Absolute permittivity is a constant that depends on the physical, chemical, and biological quality of the material, and is in fact a measure of the extent to which the material "responds" to the electromagnetic field strength. Since the response of real materials to the electric field E is time shifted, the dielectric shift D is also delayed, which can be understood as a kind of phase shift (δ). The magnitude of the phase and the phase shift itself can only be expressed in exact terms by complex numbers ($i = \sqrt{-1}$), so it is useful to express the permittivity of a given medium or material as a complex function of the frequency of the applied electromagnetic field, where ε^* is the complex permittivity:

$$\varepsilon^*(f) = \left|\frac{D}{E}\right| (cos\delta + i \, sin\delta) \tag{3}$$

As any other complex function, complex permittivity can also be separated to its real and imaginary part:

$$\varepsilon^*(f) = \varepsilon'(f) - i\varepsilon''(f) \tag{4}$$

The real part of the function is called the dielectric constant (ε'), while the complex part is called the dielectric loss factor (ε''). As can be seen from the equation above, these two quantities are frequency dependent, i.e. for a given material their values vary as a function of frequency. From an electrodynamic point of view, the dielectric constant indicates how much of the energy conveyed by the electromagnetic field can be absorbed and stored by the material interacting with it, while the loss factor expresses how much of the stored electrical energy is converted into other types of energy (such as heat or kinetic energy) [2].

The application of dielectric behaviour analysis has been broadly investigated in different disciplines, such as environmental science, biotechnology and food technology. It was shown that measuring certain dielectric parameters can be used to monitor microwave sludge disintegration and water purification [3], the efficiency of microwave-oxidation process for meat industry wastewater treatment [4], as well as to examine the process of anaerobic digestion of pre-treated sludge [5], and also in enzymatic and fermentation processes regarding lignocellulose degradation [6].

The spoilage processes of different food products are the result of microbial metabolic activities, meaning that the deterioration of these products involves a whole set of different, complex biochemical and physicochemical changes. It means that the determination of dielectric properties and their changes can be a suitable alternative for monitoring these processes. While the literature has not yet addressed in depth the monitoring of dairy product spoilage processes based on the dielectric measurement principle, research has been conducted decades ago to investigate the spoilage of other types of food products and the cell number changes of different microorganisms in terms of dielectric behaviour. In 1995, Asami and Yonezawava looked for a connection between yeast growth dynamics and dielectric properties, measuring dielectric parameters in the frequency range 0.1 to 100 MHz. The results showed that the so-called dielectric dispersion (which is actually the frequency dependence of permittivity) increased exponentially at 1 MHz in the log phase of cell number change and then stabilized in the stationary phase. This relationship clearly shows that the yeast cell count can be monitored by dielectric measurement methods [7]. In an earlier study, it was concluded that the dielectric properties of different microbial suspensions measured at radiofrequency are a direct and monotonic function of the volume fraction of the suspended phase formed by the microbial cells, i.e. the method is suitable for direct estimation of the microbial biomass size [8]. In a 1983 study, the deterioration process of real frozen food raw materials was monitored by low-frequency dielectric measurements, and the experimental raw materials were various frozen fish meat. The results of this research

led to the conclusion that the dielectric constant at 1.5 kHz was correlated with the state of spoilage of different frozen fish, while the conductivity of the test materials varied independently of spoilage [9]. In one of our earlier studies we have shown that dielectric analysis can also be used during the coagulation of raw milk: strong correlation was found between the apparent viscosity and the dielectric constant of the milk samples during the acid- and enzyme-induced coagulation of the samples [10].

The results of these earlier studies have also shown that, although the suitability of dielectric measurement as an indirect but rapid method for indicating changes in the deterioration phenomena of foodstuffs or food raw materials (e.g. microbial growth, degradation of macromolecules, etc.) has been investigated for decades, detailed microbial-specific results for a wide range of foodstuffs or raw materials are not yet available.

2. MATERIALS AND METHODS

To measure the dielectric constant, a laboratory dielectric measurement system was used. Dielectric parameters were determined using a DAK 3.5 (SPEAG GmBh) measuring sensor connected to a vector network analyser (ZVL-3 VNA, Rhode&Schwarz GmBh) with a 50-ohm coaxial power supply line. Based on my preliminary measurement results, I experienced a high level of electromagnetic interference in the upper frequency range, and therefore the tests were performed between 200 MHz and 2400 MHz. The values of the dielectric properties - dielectric constant, dielectric loss factor - as a function of frequency are obtained from the average of 3 to 3 measurements at 10 points, the arithmetic mean of which (from 30 recorded measurements) is used to determine the values of the parameters associated with a given measurement point. The spontaneous spoilage was investigated in a home-made yogurt sample, made out of raw milk. During the one-week study, the yoghurt was stored in a laboratory incubator at 20±1 °C in its original packaging in a plastic cup with a sealable snap-on lid. In addition to monitoring the storage of the yoghurt at room temperature by dielectric parameters, a microbiological test was performed. Instrumental analysis and microbiological sampling were always performed at the same time using yoghurt from the same production. For the microbiological assessment, I monitored the variation in the living Lactobacillus strain counts using MRS culture media. In the series of microbiological experiments, sampling was carried out in each measurement session by preparing 3 parallel decimal dilutions of stock solutions, from which independent decimal dilution series were formed until 106 dilution members were reached, and then inoculated onto MRS media using a spreading method as described above.

I extended the series of experiments to monitor the microbial counts of lactic acid bacteria under aerobic and anaerobic culture conditions, accordingly, half of the inoculated media were inoculated aerobically and the duplicate plates in anaerobic jars (Thermo Scientific™, Oxoid™, AnaeroJar™ 2. 5L, AG0025A) using an anaerobic modified atmosphere load (Thermo Scientific™, Oxoid™, AnaeroGen™ 2.5L Sachet, AN0025A) at 37±1 °C. After 48 h of incubation, live cell counts were determined using the formula described previously.

3. RESULTS AND DISCUSSION

During the first part of the experiment, I investigated the relationship between the changes in dielectric constant and the living cell count of *Lactobacillus* during aerobic conditions ($N_{aerobic}$; CFU/ml). Among the analysed frequencies, f=400 MHz showed the most distinct differences in the dielectric behaviour, therefore I chose this frequency value for interpreting the results. Figure 1 shows the variation of aerobic germ count and dielectric constant with time.
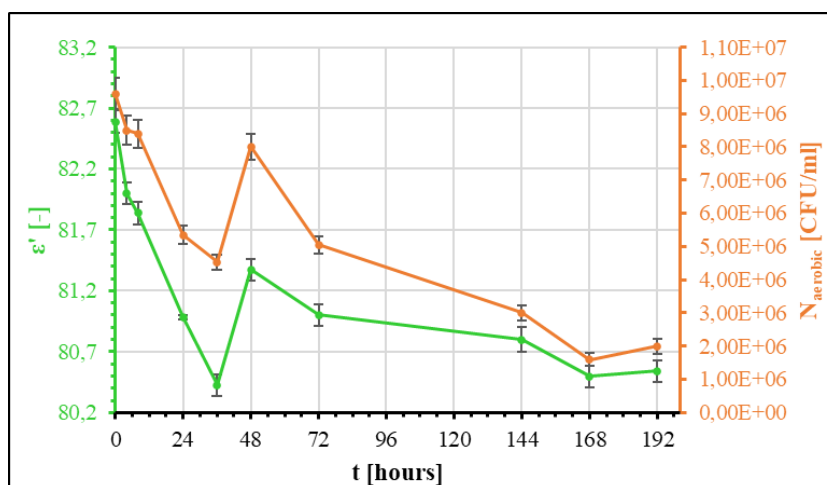
Figure 1. Changes in dielectric constant and aerobic living cell count versus time

Analysing the data, it can be seen that the number of aerobic lactic acid bacteria decreases significantly in the first 24-36 hours, almost linearly, taking into account the standard deviation, and then increases significantly between 36 and 48 hours. One possible explanation could be that the culture used for yoghurt production contained several microbial strains that initially competitively displaced lactic acid bacteria, while producing metabolic intermediates that later (36-48 hours) provided favourable conditions for their proliferation. However, further research and detailed microbiological - biochemical studies as well as further instrumental analysis are needed to explain this phenomenon precisely. A gradual decrease in the aerobic cell count was observed after 48 h, which was accompanied by organoleptic changes and the development of new microorganisms on the MRS medium used, which produced new red-pink colonies with a round morphology. It can be concluded that the deterioration of the product started on the second day of the storage experiment and that at this stage the spoilage bacteria continuously outcompeted the lactic acid bacteria.

The change in the dielectric constant, similar to previous experiments, tended to follow the cell number change, i.e. it decreased with a similar slope in the decreasing phases and increased in the increasing phase in a closely correlated manner (Figure 1). This can be explained by changes in the number of germ cells on the one hand, and by chemical and physical changes in the structure of the matrix on the other. The correlation between the two parameters was again investigated by plotting the relative cell counts and dielectric constants against the initial values (Figure 2).
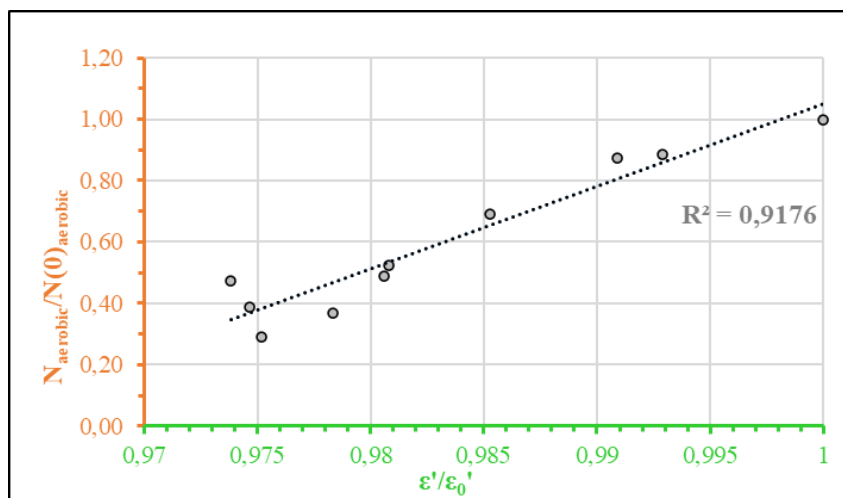
Figure 2. Correlation between the aerobic lactic acid bacteria count and the rate of change of the dielectric constant (f=400 MHz)

Figure 2 clearly shows that the correlation between cell number change and dielectric constant change is close, the coefficient of determination (R^2=0.92) indicates that the two parameters are correlated and the relationship between them is linear. In the light of the above, it can be demonstrated that the measurement of the dielectric constant can be used for this type of dairy product to provide a high level estimate of cell count change and thus indirectly to detect the spoilage process. The decreasing tendency of the dielectric constant during storage and the influence of microbial processes and the resulting pH changes during storage and spoilage (and their effects on, for example, protein structure) on dielectric behaviour were also described in a study by Szerement et al [11].

In the second phase of the research, I also investigated the connection between the dielectric constant and the anaerobic living cell counts of *Lactobacillus*. Figure 3 shows the obtained data versus time.
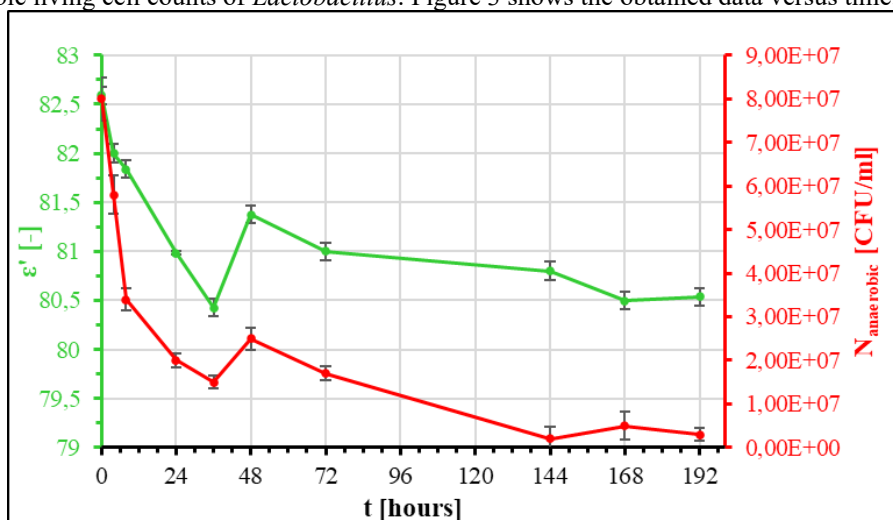

Figure 3. Changes in dielectric constant and anaerobic living cell count versus time

Examining the anaerobic lactic acid bacteria counts in the samples, phases with similar trends to the aerobic bacteria counts could be obtained, but in this case the initial decreasing phase was more pronounced, while the increasing phase between 36-48 hours was less pronounced, i.e. the lactic acid bacteria with anaerobic metabolism were less able to proliferate in the sample during this phase (Figure 3). It should be noted, however, that the anaerobic cell count was found to be inherently higher throughout the study, suggesting that a large proportion of the mixed culture used for yoghurt production had facultative anaerobic metabolism (i.e. they were able to carry out their energy-producing processes both aerobically and anaerobically), while a significant proportion of the bacteria remained viable under anaerobic conditions only, i.e. they had obligate anaerobic metabolism. After the second day, there was also a clear decline in anaerobic bacterial counts, but of a somewhat smaller slope than aerobic counts; the microbes causing the deterioration thus gradually replaced the anaerobic lactic acid bacteria in the feedstock. The change in the dielectric constant tended to follow the cell number change in this case as well, and the strength of the correlation between the two parameters is illustrated in Figure 4.
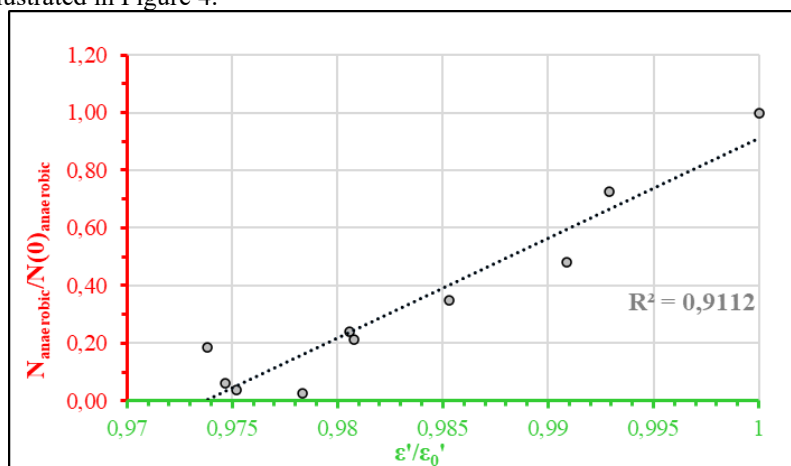

Figure 4. Correlation between the anaerobic lactic acid bacteria count and the rate of change of the dielectric constant (400 MHz)

Similar to the aerobic bacterial count change, the change in anaerobic cell count and dielectric constant values show a strong, clear correlation ($R^2 = 0.91$) and the relationship is linear.

4. CONCLUSIONS

Based on the experimental data gathered, it can be confidently stated that there is a strong correlation between changes in live cell counts of both aerobically and anaerobically cultured lactic acid bacteria and dielectric parameters. The main conclusions of the results are that the change in the bacterial count, and thus the deterioration process leading to it, can be indirectly monitored in the dairy product under study by low-frequency determination of the dielectric constant.

REFERENCES

[1] Ledenbach, L. H., & Marshall, R. T. (2009). Microbiological spoilage of dairy products. Compendium of the microbiological spoilage of foods and beverages, 41-67.
[2] Venkatesh, M. S., and G. S. V. Raghavan. "An overview of dielectric properties measuring techniques." Canadian biosystems engineering 47.7 (2005): 15-30.

[3] Kovács, P. V., Lemmer, B., Keszthelyi-Szabó, G., Hodúr, C., & Beszédes, S. (2018). Application of dielectric constant measurement in microwave sludge disintegration and wastewater purification processes. Water science and technology : a journal of the International Association on Water Pollution Research, 77(9-10), 2284–2291. https://doi.org/10.2166/wst.2018.144

[4] Jákói, Z., Hodúr, C., László, Z., & Beszédes, S. (2018). Detection of the efficiency of microwave-oxidation process for meat industry wastewater by dielectric measurement. Water science and technology : a journal of the International Association on Water Pollution Research, 78(10), 2141–2148. https://doi.org/10.2166/wst.2018.491

[5] Jákói, Z., Hodúr, C., & Beszédes, S. (2022). Monitoring the Process of Anaerobic Digestion of Native and Microwave Pre-Treated Sludge by Dielectric and Rheological Measurements. Water, 14(8), 1294. MDPI AG. Retrieved from http://doi.org/10.3390/w14081294

[6] Beszédes, S., Jákói, Z., Lemmer, B., Czupy, I. & Hodúr, C. (2020) Detection of the efficiency of enzymatic hydrolysis and fermentation processes by dielectric measurement. HUNGARIAN AGRICULTURAL ENGINEERING, 37. pp. 21-26. https://doi.org/10.17676/HAE.2020.37.21

[7] Asami K., Yonezawa T. (1995). Dielectric analysis of yeast cell growth. Biochimica et Biophysica Acta (BBA) - General Subjects. 1245(1). 99-105. DOI: 10.1016/0304-4165(95)00074-L.

[8] Harris C., Todd R. W., Bungard S. J., Lovitt R., Morris J. G., Kell D. (1987). Dielectric permittivity of microbial suspensions at radio frequencies: a novel method for the real-time estimation of microbial biomass. Enzyme and Microbial Technology. 9(3). 181-186. DOI: 10.1016/0141-0229(87)90075-5.

[9] Kent M. (1983). The effects of spoilage on the dielectric properties of frozen fish. Journal of the Science of Food and Agriculture 34(11) 1289-1296. DOI: 10.1002/jsfa.2740341119.

[10] Dobozi, R., Jákói, Z. P., Csanádi, J., & Beszédes, S. (2023). Investigating the Acid- and Enzyme-Induced Coagulation of Raw Milk Using Dielectric and Rheological Measurements. Applied Sciences, 13(10), 6185. MDPI AG. Retrieved from http://doi.org/10.3390/app13106185

[11] Szerement J., Szvplowska A., Kafarski M., Wilczek A., Lewandowski A., Skierucha W. (2018). The effect of storage time on dielectric properties of pasteurized milks and yoghurt. 2018 12th International Conference on Electromagnetic Wave Interaction with Water and Moist Substances (ISEMA). 1-9. DOI: 10.1109/ISEMA.2018.8442291.

ACKNOWLEDGEMENTS